The power of help: mechanistic insights into CD4⁺ T cell differentiation in vaccination and cancer

Bosma, D.M.T.

Chapter 5

PD-1 or CTLA-4 blockade promotes CD86-driven Treg responses upon radiotherapy of lymphocyte-depleted cancer in mice

Elselien Frijlink[1,2], Douwe M. T. Bosma[2], Julia Busselaar[2], Thomas W. Battaglia[3], Mo D. Staal[2], Inge Verbrugge[1] and Jannie Borst[2]

1 *Division of Tumor Biology and Immunology and Oncode Institute, The Netherlands Cancer Institute, Amsterdam, Netherlands.*

2 *Department of Immunology and Oncode Institute, Leiden University Medical Center, Leiden, Netherlands.*

3 *Division of Molecular Oncology and Immunology and Oncode Institute, The Netherlands Cancer Institute, Amsterdam, Netherlands.*

Published in Journal of Clinical Investigation. 2024 134(6):e171154
Doi: 10.1172/JCI171154

Abstract

Radiotherapy (RT) is considered immunogenic, but clinical data demonstrating RT-induced T-cell priming are scarce. Here, we show in a mouse tumor model representative of human lymphocyte-depleted cancer that RT enhances spontaneous priming of thymus-derived ($FOXP3^+Helios^+$) regulatory T cells (Tregs) by the tumor. These Tregs acquired an effector phenotype, populated the tumor and impeded tumor control by a simultaneous, RT-induced $CD8^+$ cytotoxic T-cell (CTL) response. Combination of RT with CTLA-4 or PD-1 blockade, which enables CD28 costimulation, further increased this Treg response and failed to improve tumor control. We discovered that upon RT, CD28-ligands CD86 and CD80 differentially affected the Treg response. CD86, but not CD80, blockade prevented the effector (e)Treg response, enriched the tumor-draining lymph node for $PD\text{-}L1^+CD80^+$ migratory, conventional dendritic cells (cDCs) and promoted CTL priming. Blockade of CD86 alone or in combination with PD-1, enhanced intra-tumoral CTL accumulation and the combination significantly increased RT-induced tumor regression and overall survival. We advise that combining RT with PD-1 and/or CTLA-4 blockade may be counterproductive in lymphocyte-depleted cancers, since they drive Treg responses in this context. However, combining RT with CD86 blockade may promote control of such tumors by enabling a CTL response.

Introduction

Immunotherapy by antibody-based immune-checkpoint blockade (ICB) is a new treatment modality for multiple cancer types. However, only a minority of patients experiences durable clinical responses[1], partially due diverse tumor immune infiltrates[2]. Recent pan-cancer transcriptome analyses have clarified immune cell compositions of most human solid cancer types and defined intra-tumoral immune cell types and states associated with good or bad prognosis[3,4]. These analyses have categorized clinically defined cancer types into subsets with different immune infiltrates[3–5]. Studies in mouse models have clarified that such infiltrates develop in dialogue between the tumor, its draining lymph nodes (dLN) and circulating immune cells[6]. Generally, tumors can either be infiltrated with T cells associated with good prognosis, or lack such T cells. In the latter case, tumors are often rich in myeloid cells and contain a bad prognosis T-cell infiltrate dominated by regulatory T cells (Tregs)[3–5]. ICB responsiveness is typically linked to tumor types infiltrated by good prognosis, effector-type $CD4^+$ and $CD8^+$ T cells[4]. Presence of good prognosis T cells in tumors depends on presence of tumor antigens, but also on favorable communication between the tumor and its dLN via conventional dendritic cells (cDCs)[7]. This communication is primarily shaped by tumor genetics, including oncogenic driver pathways[8].

Interventions should elicit de novo T-cell responses to achieve clinical benefit in cancers devoid of effector T-cells[9]. In attempts to accomplish this, ICB is combined with radiotherapy (RT) in multiple clinical trials[10]. This combination is attractive for multiple reasons: 1) RT-induced tumor cell death reduces tumor burden, potentially relieving systemic immune suppression, 2) RT can modulate the tumor micro-environment (TME), making it more permissive for T cell-mediated tumor destruction[11], and 3) RT can support systemic anti-tumor immunity by generating new tumor-specific T-cell responses in the tumor-dLN (TdLNs), a process called T-cell priming. It is proposed that RT can prime systemic anti-tumor T-cell responses, based on theory and observations in mouse models[12–14]. Upon RT-induced tumor cell destruction, cell debris is released, containing tumor-derived antigens and danger-associated molecular patterns (DAMPs)[15]. Locally, migratory cDCs engulf this debris, migrate to TdLNs and initiate T-cell responses. To prime $CD8^+$ T cells, the cDC1 subset is required that excels in cross-presenting peptides from phagocytosed proteins in MHC class I (MHC-I) molecules. Activated cDC1s also provide specific costimulatory and cytokine signals, instructing $CD8^+$ T cells to expand and differentiate into competent cytotoxic T lymphocytes (CTLs)[16]. The potential of RT to induce a systemic T-cell response predicts that it may potentiate abscopal effects, i.e. tumor regression outside the field of radiation. Clinically, such observations are extremely rare[17], indicating impediments in this process[11]. In certain immunogenic mouse tumor models, RT can induce T-cell infiltration of the irradiated tumor, as well as an "abscopal" tumor implanted on a non-irradiated site in the same mouse[18–20].

However, clinical effects of combining RT with CTLA-4 or PD-1 targeting ICB are disappointing[10,21–24]. For example, RT as induction treatment did not enhance PD-1 blockade efficacy in metastatic triple negative breast cancer patients, nor did it improve T-cell infiltration in the TME[21]. We propose that the immune cell composition of the tumor, as dictated by its dialogue with the TdLN, is decisive for the success of RT/ICB combinations. Certain mouse tumor models spontaneously become infiltrated with tumor-specific effector T-cells and regress upon RT alone[25], or in combination with ICB[26], without requiring de novo T-cell priming. In such T-cell infiltrated tumors, RT apparently enables tumor-infiltrated T cells to exert their effector functions locally. However, in lymphocyte-depleted tumor types that lack pre-existing tumor-specific effector T-cells, RT must induce new T-cell priming to enable T-cell mediated tumor control. Lack of antigens, insufficient cDC activating signals[27] and/or tumor-imposed immunosuppression can hamper this process[28].

In this study, we delineate how the T-cell response to RT may proceed in lymphocyte-depleted cancers. For this purpose, we defined a mouse tumor model representing human lymphocyte-depleted cancer by bioinformatic analysis and used it for detailed analysis of RT-induced T-cell immunity and impact of ICB. We found that this tumor type spontaneously induced priming and tumor infiltration by effector phenotype, thymus-derived ($FOXP3^+Helios^+$) Tregs, which was exacerbated by RT and prevented CTL-mediated tumor control. Counterintuitively, antibody-mediated blocking of co-inhibitory receptors CTLA-4 or PD-1 further increased this Treg response and antagonized tumor regression.

Recent work has indicated that both CTLA-4 and PD-1 blockade enable CD28 costimulation of T cells. CD28 signals amplify T-cell receptor (TCR)/CD3 signals to promote expansion of newly activated $CD4^+$ and $CD8^+$ T cells[29]. CTLA-4 is constitutively expressed on Tregs and downregulates the CD28-ligands CD80 and CD86 on cDCs[30]. Therefore, CTLA-4 attenuates the ability of cDCs to induce CD28 costimulation of conventional, non-regulatory T cells (Tconvs)[30]. PD-1 is associated with the SHP2 tyrosine phosphatase that extinguishes CD28 signals in cis[31]. Thus, CTLA-4 and PD-1 use different mechanisms, but both control T-cell responses by suppressing CD28 costimulation. We discovered that in the lymphocyte-depleted cancer model, CD28 costimulation enabled by ICB, drove the RT-induced Treg response. Selective blockade of the CD28-ligand CD86 inhibited the Treg response and promoted CTL priming and tumor control. We therefore advise that combining RT with PD-(L)1 and/or CTLA-4-targeting ICB can be counterproductive in lymphocyte-depleted cancers and identify CD86 as an alternative target for ICB in such cases.

Results

RT response is deficient in T-cell depleted human tumor types

To identify how the tumor immune cell composition influences RT responses in human cancer, we examined the relationship between immune phenotype and RT efficacy in a wide variety of human cancers. Using records from The Cancer Genome Atlas (TCGA), we identified five previously characterized pan-cancer immune phenotypes[3] in patients for which RT status was specified (**Supplementary Figure 1, A and B**). These immune phenotypes are described as "wound healing" (C1), "IFNg dominant" (C2), "inflammatory" (C3), "lymphocyte depleted" (C4) and "immunologically quiet" (C5). While RT had a positive effect on overall survival (OS) in tumors classified as C1-3 immune subtypes, RT had a negative effect on OS in the C4 and C5 subtypes (**Figure 1A**) that are identified by low lymphocyte- and high myeloid cell content[3]. The remarkably defective response to RT of tumors with a C4 and C5 immune phenotype prompted us to examine the underlying mechanism.

We set out to find a mouse tumor model with a C4/C5-like lymphocyte-depleted phenotype. We trained a K-nearest neighbor (KNN) classifier to distinguish between the C3 versus C4/C5 immune subtypes (**Supplementary Figure 1C**) and subsequently applied our model to microarray data of murine (C57BL/6)-derived MC38 and TC-1 tumor models[32]. We found similarity between the colon carcinoma cell line MC38 and the C3 subtype and between the lung carcinoma cell line TC-1 and the C4/5 subtype (**Figure 1B**). Although both tumors express non-self antigens[33,34], the MC38 tumor is immunogenic and raises a high T-cell infiltrate[20], whereas the TC-1 tumor does not[35]. In agreement, MC38 is responsive to ICB[36], whereas TC-1 is not[37]. Accordingly, flow cytometry analysis revealed a significantly lower proportion of $CD8^+$ T cells in TC-1 tumors as compared to MC38 tumors (**Figure 1C**).

We assessed how MC38 and TC-1 tumors respond to RT, using three consecutive doses of 8 Gy (3x 8 Gy) or a single dose of 20 Gy, regimens that are immune stimulatory in mouse tumor models[12,38]. Both regimens led to MC38 tumor control but were much less effective in TC-1 tumor control (**Figure 1D**). This agrees with the finding that the pre-existing T-cell infiltrate in the MC38 tumor contributes to the RT response[25] and suggests impediments for immune-mediated control of the TC-1 tumor upon RT. We therefore continued our study with the TC-1 tumor to examine the RT-induced T-cell response in this representative model of lymphocyte-depleted cancer.

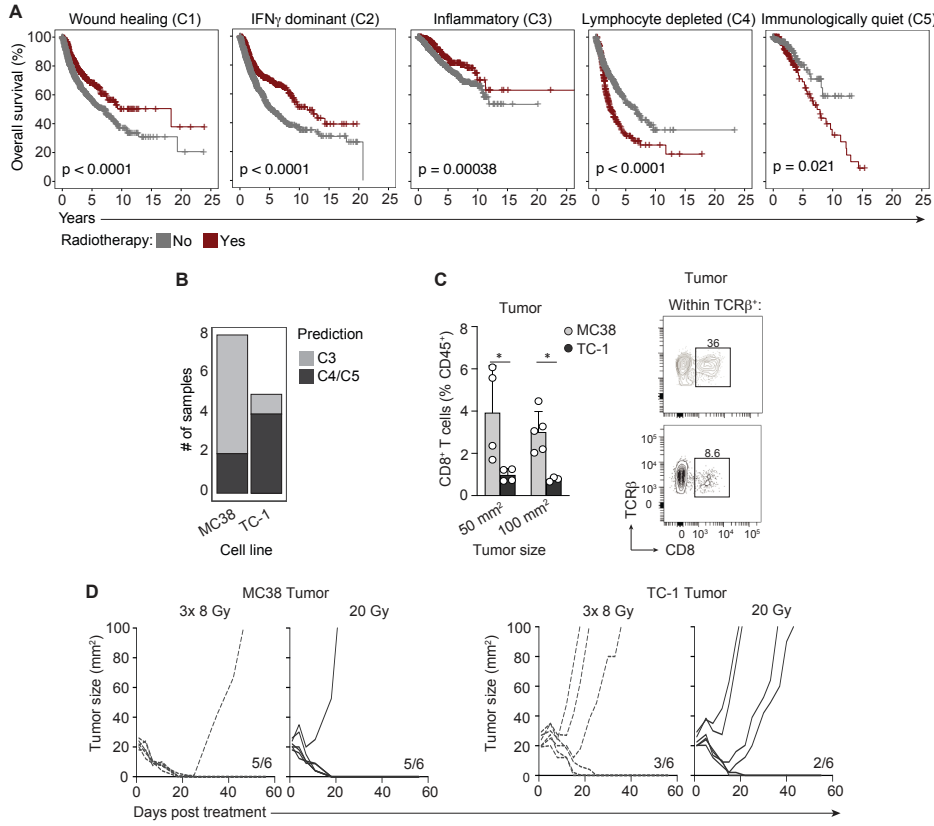

Figure 1. Lymphocyte-depleted (C4/5) human cancers have suboptimal response to RT and are modelled by the murine TC-1 tumor.

(A) Kaplan-Meier overall survival curves obtained from TCGA for patients receiving RT (red) or not (grey) within the C1 "wound healing" (n=2136), C2 "IFNg dominant" (n=2296), C3 "inflammatory" (n=1903), C4 "lymphocyte depleted" (n=1055) and C5 "Immunologically quiet" (n=354) cancer immune subtypes. Log-rank p-values were generated using a Cox proportional-hazards model. **(B)** C3 "inflammatory" versus C4/C5 "lymphocyte depleted" model predictions from transcriptome data of C57BL/6- syngeneic MC38 and TC-1 transplantable tumors. **(C)** Frequency of $CD8^+$ T cells among $CD45^+$ cells in MC38 (total n=9) and TC-1 (total n=7) tumors measured at the indicated tumor sizes (left), and representative flow cytometry plots (right) depicting the percentage of $CD8^+$ T cells within $TCRb^+$ cells in 50 mm^2 MC38 (grey) and TC-1 (black) tumors. **(D)** Tumor growth curves of MC38 (n=6/group, left) and TC-1 (n=6/group, right) tumor-bearing mice treated with either 8 Gy over 3 days (3x 8 Gy) or a single dose of 20 Gy RT. Ratios indicate the number of mice out of total treated that showed full recovery upon RT. Error bars indicate SD. *P < 0.05, Mann-Whitney test.

Despite high myeloid and Treg cell content, the RT response of TC-1 is CD8$^+$ T-cell dependent

In the TME of the TC-1 tumor, the T-cell compartment, consisting of CD8$^+$ and CD4$^+$ Tconvs and FOXP3$^+$ Tregs, comprised only 11.1% of the CD45$^+$ hematopoietic cell infiltrate, as identified by flow cytometry. Conversely, myeloid cells comprised 62.5% of the CD45$^+$ cell infiltrate, including macrophages and neutrophils (**Figure 2A, Supplementary Figure 2A**), consistent with a myeloid-rich, T-cell devoid phenotype[4,5]. The association between Treg and (suppressive) myeloid cell infiltrates is well described and often linked to (systemic) immunosuppression[6]. To characterize the T cell population, we performed detailed spectral flow cytometry analysis of the CD3$^+$ lymphocyte population in the tumor, TdLNs and non-TdLNs. FlowSOM-guided clustering analysis and Uniform Manifold Approximation and Projection (UMAP)-dimension reduction (**Supplementary Figure 2, B and C**) identified seven main clusters, including CD8$^+$ and CD4$^+$ (FOXP3$^-$) Tconvs, proliferating (Ki67$^+$) CD8$^+$ and CD4$^+$ T cells, central (c) Tregs, effector (e)Tregs and CD4$^-$/CD8$^-$ T cells. The Tregs that prevent auto-reactive Tconv responses at steady state originate in the thymus and reside in secondary lymphoid organs as cTregs. In response to antigen and inflammatory signals, cTregs can expand and differentiate into eTregs that populate peripheral tissues to dampen inflammation[39]. The eTreg population was proliferating and had high expression of the effector marker ICOS, alongside steady-state Treg markers FOXP3, CTLA-4 and CD25. Co-expression of the transcription factor Helios indicated that these eTregs are thymus-derived, and not peripherally induced Tregs resulting from the conversion of Tconvs into Tregs[40]. eTregs displayed high expression of CD44 and lacked CD62L (**Figure 2C, Supplementary Figure 2D**), confirming their effector phenotype[39]. Unlike the eTregs, cTregs, as defined in the TdLN, expressed CD62L, did not proliferate, had no ICOS expression and lower expression of the Treg markers (**Figure 2, B and C, Supplementary Figure 2D**). Helios was expressed in over 70% of cTregs and this was further enriched in eTregs in both naïve and TdLNs (**Figure 2D, Supplementary Figure 2D**). Quantification of the identified populations revealed no increase in proliferating CD8$^+$ or CD4$^+$ Tconvs in LNs upon TC-1 tumor outgrowth (**Supplementary Figure 2E**). However, compared to naïve mice, the frequency of eTregs – but not cTregs – in the TdLN was significantly increased in tumor-bearing mice and eTregs were also present in the tumor (**Figure 2E**). Importantly, the Treg population in the tumor has overall a CD44^{high}CD62L$^-$ effector phenotype (**Supplementary Figure 2D**), but based on low levels of ICOS and CTLA-4 and lack of proliferation, they cluster as cTregs (**Supplementary Figure 2, B-D**). These data suggest that during its outgrowth, the TC-1 tumor stimulates expansion and differentiation of Tregs in the TdLN, and these cells also populate the tumor, underscoring the communication between the tumor and TdLN[6,41].

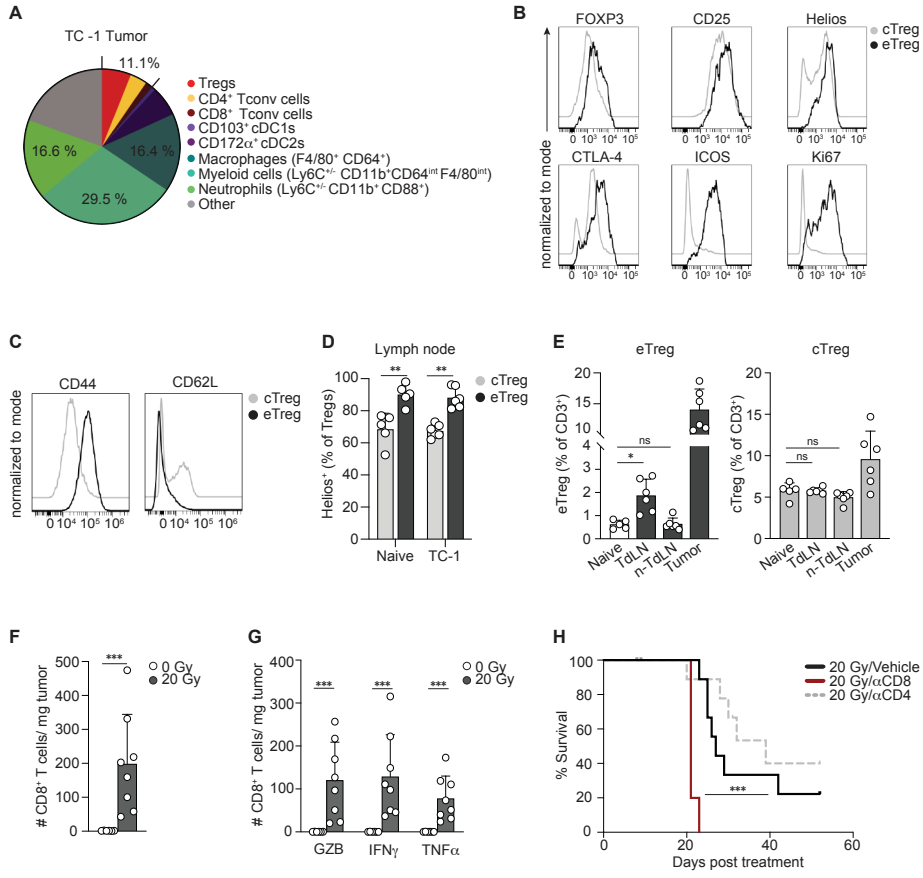

Figure 2. Myeloid- and Treg cell-rich TC-1 tumor shows CD8⁺ T-cell dependent RT response.
(A) Frequency of the indicated immune cell populations among CD45⁺ cells measured by flow cytometry in 50 mm² TC-1 tumors (n=6). **(B-D)** cTregs and eTregs were defined as indicated in **Supplementary Figure 2, B-D** and identified in TdLN, non-TdLN and tumor of 100 mm² TC-1 tumor-bearing (n=6) and age-matched naïve (non tumor-bearing) mice (n=5). FlowSOM guided clustering was performed on 5000 randomly selected cells per sample within the CD3⁺ lymphocyte population. **(B, C)** Representative histograms depicting expression of indicated markers on cTreg and eTreg populations in axillary LNs of naïve and TC-1 tumor bearing mice. **(D)** Frequency of Helios⁺ cells among cTregs and eTregs in axillary LNs of naïve and TC-1 tumor bearing mice. **(E)** Percentage of eTregs (left) and cTregs (right) among CD3⁺ cells in the indicated tissues. **(F-H)** Monitoring by flow cytometry of the CD8⁺ T-cell response to 20 Gy RT (n=8) or control (0 Gy, n=6) in TC-1 tumors. **(F)** Absolute number (#) of total CD8⁺ T cells or **(G)** granzyme B (GZB), IFNg, or TNFa-expressing CD8⁺ T cells per milligram (mg) tumor tissue at day 8 post RT. IFNg and TNFa were measured after *in vitro* PMA/Ionomycin stimulation. **(H)** Overall survival of TC-1 tumor-bearing mice treated with 20 Gy RT at day 0 in combination with vehicle (PBS, n=9) or depleting mAbs specific for CD8⁺ (n=5) or CD4⁺ (n=9). ***P < 0.001 (Mantel-Cox analysis). Data are from one experiment representative of at least two experiments. Error bars indicate SD. *P < 0.05, *** P < 0.001, Kruskal-Wallis test with uncorrected Dunn's post hoc analysis in **E**, Mann-Whitney test in **D, F** and **G**. ns; no significance.

Importantly, RT with either 20 Gy or 3x 8 Gy significantly augmented the absolute number of $CD8^+$ T-cells in the TC-1 tumor (**Figure 2F, Supplementary Figure 3A**). These tumor-infiltrating $CD8^+$ T cells were functional CTLs, as evidenced by the expression of Granzyme B (GZB) and the effector cytokines IFNg and TNFa (**Figure 2G**). Both RT regimens also increased the absolute number of ($FOXP3^-$) $CD4^+$ Tconvs, albeit to a lesser extent than $CD8^+$ T cells (**Supplementary Figure 3B**). Systemic depletion of $CD8^+$ T cells, but not of $CD4^+$ T cells, significantly reduced RT-induced mouse survival (**Figure 2H**, **Supplementary Figure 3, C-E**), arguing that the RT-induced CTL response makes a major contribution to control of the TC-1 tumor by RT. This finding suggests that there might be a window of opportunity to improve RT-induced, CTL-mediated control of lymphocyte-depleted cancers.

RT of the TC-1 tumor induces CTL priming, next to a Treg response that limits tumor control

The influx of effector CTLs in the irradiated TC-1 tumor likely originated from the induction of a de novo $CD8^+$ T-cell response in the TdLN by RT[15]. In certain immunogenic mouse models, T-cell priming proved important for durable RT-induced anti-tumor immunity[12,13]. To visualize new T-cell priming after RT of the TC-1 tumor, mice were treated with the S1P-receptor agonist FTY720, which traps T cells in LNs[42]. This enlarges the window to identify newly primed T cells in the TdLN. FTY720 efficacy was confirmed by the elimination of circulating $CD8^+$ and $CD4^+$ T cells in peripheral blood (**Supplementary Figure 4A**). Treatment with FTY720 did not affect tumor development (**Supplementary Figure 4B**). At day 8 after RT, T-cell priming and effector differentiation were analyzed in the TdLN. The flow cytometry panel included the transcription factor TCF-1 to monitor CTL effector differentiation[43]. TCF-1 loss signifies reduced "stemness"[44] and a shift towards more differentiated effector T cells[43]. In presence of FTY720, a significant RT-induced increase in effector phenotype $CD44^+$ $TCF\text{-}1^-$, GZB^+- and $IFNg^+$ expressing $CD8^+$ T cells was revealed (**Figure 3, A and B**), while the effect of RT on effector phenotype $CD4^+$ T cells was less pronounced (**Supplementary Figure 4C**). Moreover, FTY720 treatment revealed that a large part of the effector $CD8^+$ T cells present in the tumor after RT originated from the TdLN, since their frequency in the tumor was significantly reduced upon FTY720 treatment (**Figure 3, C and D**). This was not evident for effector $CD4^+$ T cells (**Supplementary Figure 4D**). Thus, in the lymphocyte-depleted TC-1 tumor model, RT elicits priming of $CD8^+$ T cells that subsequently migrate into the irradiated tumor.

Despite RT-induced CTL priming, not all TC-1 tumor-bearing mice were cured (**Figure 1D**). Since the TC-1 tumor induced Treg priming during its development, and because of the described increase of Tregs in the TME upon RT[28,45,46], we considered that RT might enhance the Treg response in the TC-1 tumor setting. Tregs reportedly

require antigen-dependent activation and expansion in the TdLN prior to migration to a tumor[41,47]. Treg frequencies (**Figure 3E, Supplementary Figure 4E**) and absolute numbers (**Supplementary Figure 4F**), were significantly increased in TdLN and tumor, but not in the non-TdLN, at day 8 after RT. In addition, overall Treg frequency was increased in blood over time (**Figure 3F**), and the frequency of proliferating ($Ki67^+$) Tregs was enhanced in the TdLN but not in the non-TdLN following RT (**Supplementary Figure 4, G and H**). In contrast, the frequency of proliferating Tregs in the TME was significantly decreased upon RT (**Supplementary Figure 4, G and H**). These data suggest that RT induced Treg priming in the TdLN, followed by migration of these cells into the irradiated TME, rather than RT-induced Treg expansion in the TME[45]. FTY720 treatment supported this observation, since the Treg frequency was increased in the TdLN after RT, while the frequency of Tregs in the TME was decreased (**Figure 3G**). FTY720 treatment also led to an increased Treg frequency in the TdLN of control mice (0 Gy). These data show that TC-1 tumor development induces priming and tumor infiltration by Tregs and this is exacerbated by RT.

Thus, RT promoted the Treg response next to inducing a new $CD8^+$ T-cell response, which significantly lowered the $CD8^+$ T cell/Treg ratio in the TdLN and maintained the unfavorable $CD8^+$ T cell/Treg ratio in the tumor (**Figure 3H**). Therefore, Tregs might be an impediment to CTL-mediated tumor control upon RT. To test this, we treated mice with an Fc-modified antibody to CD25[48] that efficiently depleted peripheral and intra-tumoral Tregs (**Supplementary Figure 5, A and B**) but not $CD8^+$ or $CD4^+$ Tconvs (**Supplementary Figure 5C**), both before and after RT (**Supplementary Figure 5D**). This treatment greatly improved TC-1 tumor control and overall survival (**Figure 3I, Supplementary Figure 5E**). A 3x 8 Gy RT regimen gave similar results (**Supplementary Figure 5, F and G**). Taken together, these data indicate that in the TC-1 tumor model, Tregs limit RT-mediated tumor eradication, likely by inhibiting the RT-induced CTL response.

CTLA-4 blockade increases the RT-induced Treg response and does not improve tumor control

CTLA-4 blockade has been shown to enhance RT-induced tumor regression in mouse models[49,50] and clinical studies[22,23,51]. To evaluate the effects of CTLA-4 blockade in our lymphocyte-depleted TC-1 tumor model, we treated tumors with RT and administered a blocking antibody to CTLA-4, that does not deplete Tregs[52,53], or vehicle on successive days. Anti-CTLA-4 treatment did not improve RT-induced TC-1 tumor control or overall survival (**Figure 4, A and B**). Interestingly, CTLA-4 blockade increased the RT-induced Treg response in both TdLN and non-TdLN, and the Treg population remained high in the tumor (**Figure 4C**). The majority of these Tregs expressed Helios (**Supplementary Figure 6, A and B**), indicating that RT and CTLA-4 blockade promote the response of

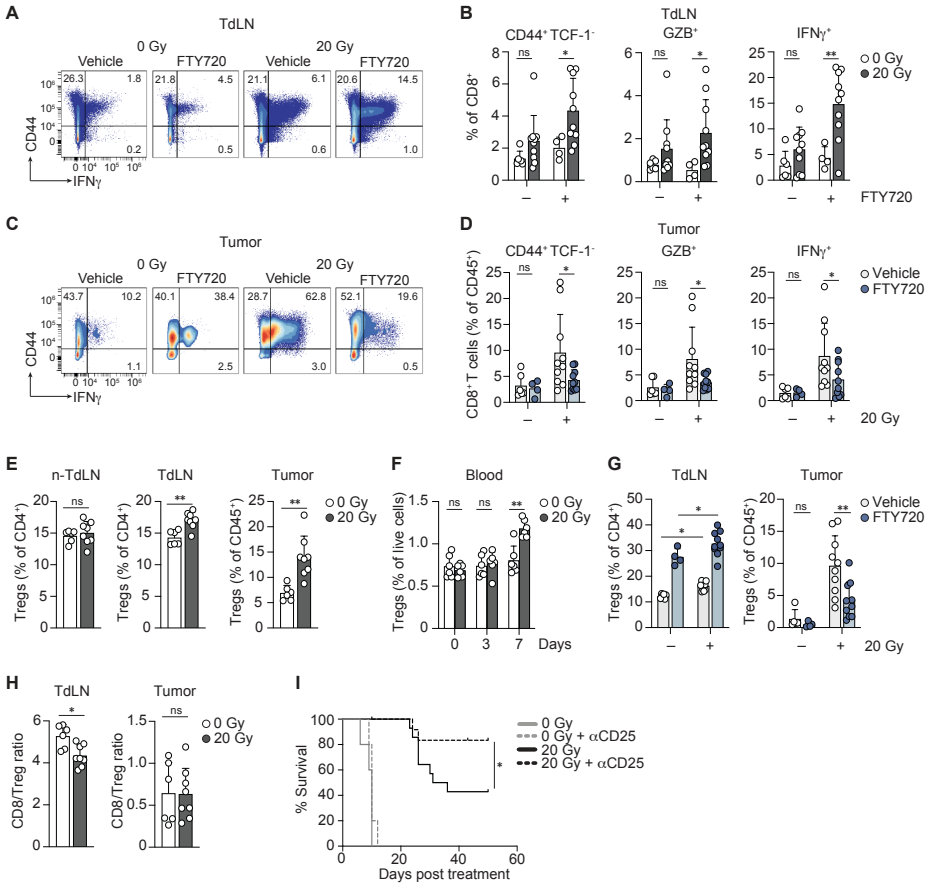

Figure 3. RT induces concomitant CTL- and Treg responses in the TC-1 tumor model.
(A-D) TC-1 tumor-bearing mice were treated with 20 Gy RT (n=10) or control (0 Gy, n=4-6) when tumors reached ~20 mm² (day 0). FTY720 or vehicle (NaCl) was administered orally on days -1, 3 and 5. On day 8, the $CD8^+$ T-cell response was analyzed by flow cytometry in TdLN **(A,B)** and tumor **(C,D)**. **(A,C)** Representative concatenated flow cytometry plots showing $IFN\gamma^+$ cells among $CD8^+$ T cells in TdLN **(A)** and tumor **(C)**. **(B,D)** Frequency of $CD44^+TCF\text{-}1^-$, GZB^+ and $IFN\gamma^+$ cells among $CD8^+$ T cells in the TdLN **(B)** and tumor **(D)**. IFNγ was measured after *in vitro* PMA/Ionomycin stimulation. **(E,F)** Monitoring of the ($FOXP3^+$ $CD25^+$) Treg response to 20 Gy RT (n=6-8) or control (0 Gy, n=6) in TC-1 tumor-bearing mice at day 8 post-treatment. **(E)** Treg frequency among $CD4^+$ T cells in the non-TdLN and TdLN, or among $CD45^+$ cells within the tumor. **(F)** Percentage of Tregs among live cells in blood at the indicated time points (n=6/group). **(G)** Frequency of Tregs in indicated tissues on day 8 following 20 Gy (n=10) or control (0 Gy, n=4-6) with or without FTY720 treatment. **(H)** $CD8^+$ T cell-to-Treg cell ratio in TdLN and tumor post-RT. **(I)** Overall survival of TC-1 tumor-bearing mice treated with 0 Gy (n=5) or 20 Gy RT (n=11-14/group) in combination with a CD25-depleting mAb or vehicle (PBS) administered I.P. on days -1 and 5 post-RT. *P < 0.05 (Mantel-Cox analysis). Data are from one experiment representative of at least two experiments. Error bars indicate SD. *P < 0.05, **P < 0.01, *** P < 0.001, **** P < 0.0001, two-way Anova with Bonferroni's post hoc test in **B, D, F** and **G**, Mann-Whitney test in **E**, and **H**. ns; no significance.

thymus-derived Tregs. To more comprehensively characterize how CTLA-4 blockade affected the T-cell response, we performed FlowSOM-guided clustering analysis and dimensionality reduction on the $CD3^+$ populations in the different tissues (**Figure 4, D and E, Supplementary Figure 6C**). CTLA-4 blockade in context of RT significantly increased the frequencies of both eTregs and cTregs in the non-TdLN and TdLN, as compared to RT alone (**Figure 4, F and G**). RT as a single treatment selectively increased the proportion of eTregs, but not of cTregs, in the TdLN (**Figure 4G**), suggesting that RT is required to facilitate cTreg to eTreg conversion. In the tumor, RT alone and in combination with CTLA-4 blockade increased the eTreg frequency (**Figure 4G**). FTY720 treatment revealed that CTLA-4 blockade supported RT-induced Treg expansion in the TdLN, rather than inducing Treg expansion in the TME (**Figure 4H**, **Supplementary Figure 6D**)[53]. Specifically, the Tregs migrated from TdLN to the tumor, as shown by the strong reduction in Treg frequency in the tumor after FTY720 treatment.

Thus, the TC-1 tumor promotes priming of thymus-derived Tregs in the TdLN and RT, alone and in combination with CTLA-4 blockade further support this process. Subsequently, these newly primed Tregs populate the tumor. Tregs are highly dependent on CD28 costimulation for their expansion[54,55]. Due to the prevalence of Tregs in the TdLN of the TC-1 tumor, CTLA-4 blockade may favor Treg over Tconv responses. Tregs may capitalize on the increased availability of CD80 and/or CD86 on cDCs following CTLA-4 blockade, leading to enhanced CD28 costimulation and subsequent Treg priming (**Figure 4I**).

CD86 rather than CD80, promotes the RT-induced Treg responses

The findings above highlight the importance of the CD28 costimulatory axis in regulating Treg expansion. They raise the possibility that the CD28 ligands CD80 and/or CD86 may dictate Treg numbers after RT in the TC-1 tumor model. We therefore selectively blocked CD80 or CD86 in presence of RT and examined the T-cell response in detail by spectral flow cytometry as before (**Figure 5, A and B**). Interestingly, CD86 blockade significantly reduced the RT-induced eTreg population in non-TdLN, TdLN and tumor (**Figure 5, C and D**). After CD86 blockade, the frequencies of eTregs in these tissues were comparable to those in non-irradiated mice (0 Gy). CD86 blockade diminished the proportion of cTregs to some extent in the non-TdLN but not in the TdLN. In contrast, CD80 blockade in the context of RT only reduced the frequency of eTregs in the TdLN (**Figure 5, C and D**). Thus, in the TC-1 tumor setting, CD86 is the selective CD28-ligand that supports the generation of an eTreg response after RT (**Figure 5E**).

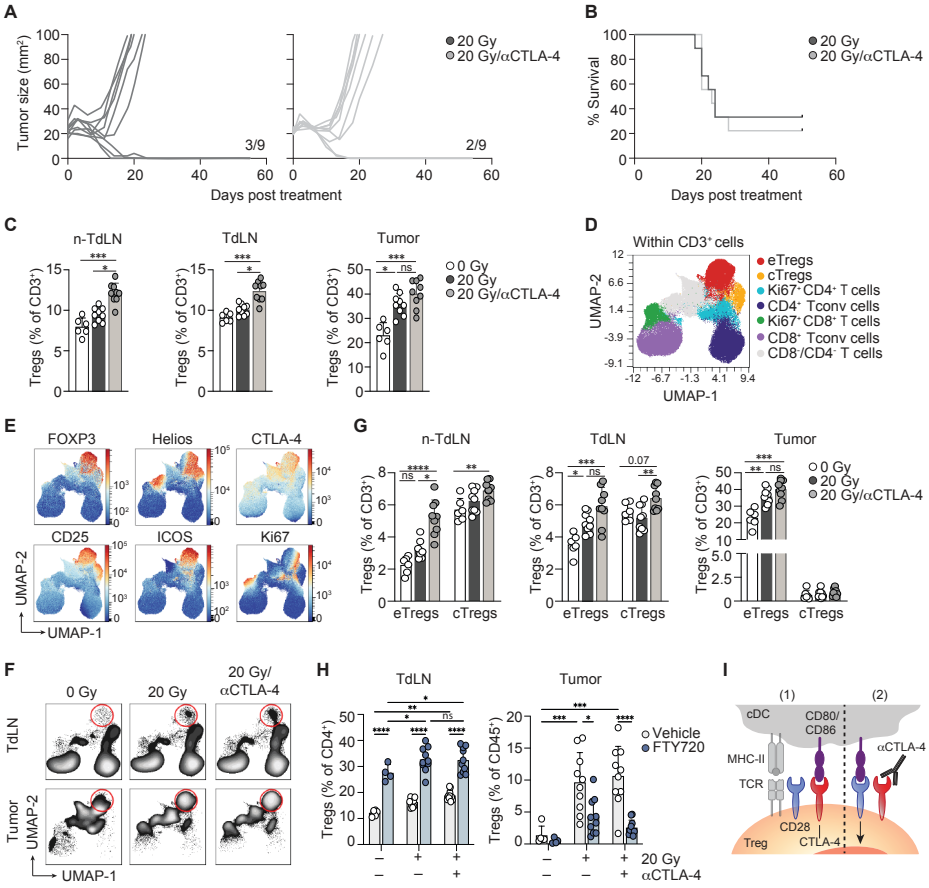

Figure 4. CTLA-4 blockade exacerbates RT-induced eTreg expansion.
Mice bearing 20 mm² TC-1 tumors received RT (20 Gy, n=9) or control (0 Gy, n=6) on day 0. Treatment included vehicle (PBS) or a CTLA-4 blocking mAb on day 0, 3, 6 and 9, with longitudinal monitoring **(A, B)** and flow cytometric analysis of the non-TdLN, TdLN and tumor on day 8 post-treatment **(C-G)**. **(A)** Individual tumor growth curves and **(B)** overall survival of the treatment groups. Ratios indicate the number of mice that showed full recovery upon treatment compared to total. **(C)** Percentage of total Tregs among CD3⁺ lymphocytes in the indicated tissues at day 8. **(D-F)** UMAP display of 2500 randomly selected CD3⁺ cells per sample in non-TdLN, TdLN, and tumors on day 8 for all treatment groups combined, with FlowSOM guided clustering (see also **Supplementary Figure 2B) (D)** and marker visualization **(E)** used to highlight the eTreg response. (**F)** UMAP visualization of the response of the CD3⁺ subpopulations in TdLN and tumor to the indicated treatments. The circles highlight the eTreg population. **(G)** Frequencies of eTregs and cTregs identified in **(D)** among CD3⁺ cells found in the indicated tissues on day 8 post treatment. **(H)** TC-1 tumor-bearing mice received 20 Gy (n=10/group) or control (0 Gy, n=4-6), with CTLA-4 mAb blockade or vehicle on days 0, 3, and 6, with or without FTY720. Treg frequency measured in TdLN and tumor on day 8 post-RT. (Same experiment as Figure 3G). **(I)** Visual representation of how Tregs benefit from CTLA-4 blockade. Data are from one experiment representative of two experiments. Error bars indicate SD. *P < 0.05, **P < 0.01, *** P < 0.001, **** P < 0.0001, Kruskal-Wallis with Dunn's post hoc test in **C** and **G**. Two-way Anova with Tukey's multiple comparisons test in **H**. ns; no significance.

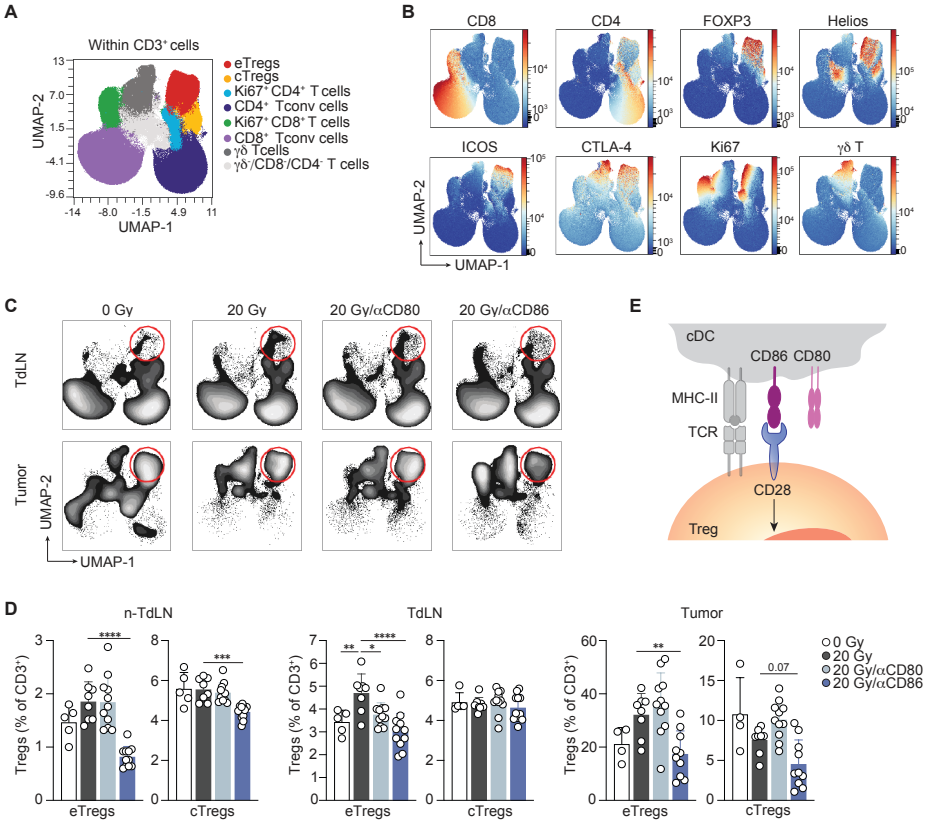

Figure 5. CD86, but not CD80, drives the RT-induced eTreg response.
Mice bearing 20 mm^2 TC-1 tumors received control treatment (0 Gy, n=5) or 20 Gy RT at day 0 in combination with either vehicle (PBS, n=8) or blocking mAb against CD80 (n=11) or CD86 (n=11) at day 0, 3 and 6. The CD3$^+$ lymphocyte response was monitored by flow cytometry in the non-TdLN, TdLN and tumor at day 8. **(A-C)** UMAP visualization of 2500 randomly selected CD3$^+$ cells per sample found in non-TdLN, TdLN and tumors at day 8 of all treatment groups combined. FlowSom guided clustering **(A)** identifying the same populations as found in the previous figures and **(B)** representative heat maps of the markers included to determine the CD3$^+$ subpopulations. **(C)** Visualization of the response of the CD3$^+$ subpopulations in TdLN and tumor to the indicated treatments. The circles highlight the eTreg population. **(D)** Frequencies of eTregs and cTregs identified in **(B)** among CD3$^+$ cells found in the indicated tissues at day 8 post treatment. **(E)** Graphic visualization of how CD86, but not CD80, binds CD28 to support Treg expansion. Data are from one experiment representative of two experiments. Error bars indicate SD. *P < 0.05, **P < 0.01, *** P < 0.001, **** P < 0.0001, ordinary one-way Anova with Dunnett's post hoc test in **D**.

CD86 blockade in context of RT improves conventional (c) DC costimulatory status and CTL priming

To clarify how CD80/CD86 blockade impacted T-cell priming, we examined migratory cDC1 and cDC2, which are responsible for T-cell priming[56–58], using flow cytometry (**Supplementary Figure 7A**). The absolute number of cDC1s or cDC2 in the TdLN remained unchanged with RT alone as compared to control. However, the combination of RT with CD86 blockade significantly increased cDC1 numbers, and there was a similar trend for cDC2s (**Figure 6A**). CD86 is constitutively expressed on cDCs, while CD80 is upregulated upon activation[29]. In the context of RT, CD86 blockade significantly increased CD80 expression on both cDC1s and cDC2s, while CD86 expression remained unaffected (**Supplementary Figure 7, B and C**). CD86 and CD80 blockade had no significant impact on CD40 or PD-L1 expression on either cDC1s or cDC2s (**Supplementary Figure 7, B and C**).

On cDCs, CD80 can form a heterodimer with PD-L1. This CD80:PD-L1 heterodimer engages CD28, but cannot bind to PD-1, nor can it be downregulated by CTLA-4[59,60]. Co-expression of CD80 and PD-L1 on cDCs positively correlates with enhanced CTL priming capacity against cancer, in agreement with increased formation of a CD28-costimulatory CD80:PD-L1 heterodimer[61]. In the TC-1 tumor model, the frequency of cDC1s and cDC2s co-expressing CD80 and PD-L1 was significantly increased when RT was combined with CD86 blockade (**Figure 6, B-D**). The frequency of $CD80^+$ $PD\text{-}L1^-$ cells was also increased, whereas the frequency of $CD80^-$ $PD\text{-}L1^+$ cells was decreased. Thus, in the TC-1 model, RT induced CTL priming is likely increased upon CD86 blockade by increasing the frequency and costimulatory state of migratory cDC1s that present tumor antigen in the TdLN.

To study CTL priming, we performed opt-SNE analysis of $CD8^+$ T cells with a $CD44^+$ $CD62L^-$ effector phenotype found in the TdLN. Contour plot visualization revealed that the $TCF\text{-}1^-$ subpopulation among $CD44^+CD62L^-$ cells in the TdLN was significantly enlarged after RT, and further increased upon combined treatment with CD86, but not CD80, blockade (**Figure 6, E and F**). Manual gating (**Supplementary Figure 7D**) confirmed these findings and showed that CD86 blockade in the context of RT significantly increased the frequency of $CD44^+TCF\text{-}1^-$ cells among $CD8^+$ T cells in both TdLN and tumor (**Figure 6G**). Phenotypical analysis also showed increased expression of the effector differentiation markers CD43, CX3CR1, GZB and KLRG1 on the $CD44^+$ $TCF\text{-}1^-$ $CD8^+$ T cell population as compared to the $CD44^+TCF\text{-}1^+$ population (**Figure 6H**). Moreover, the frequency of $Ki67^+CD44^+TCF\text{-}1^-$ cells was increased, indicating increased cell cycle activity (**Figure 6H**). The collective findings indicate that CD86 blockade improves RT-induced CTL priming, expansion and effector differentiation, likely facilitated by increased presence of costimulatory migratory cDC1s in the TdLN.

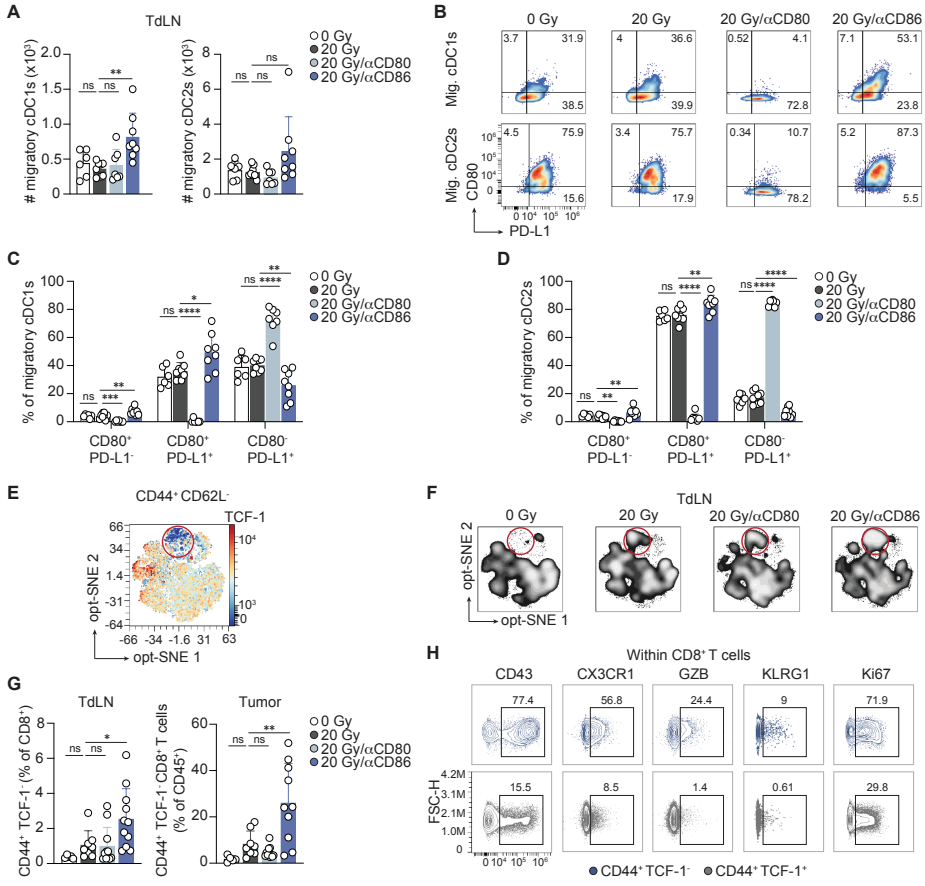

Figure 6. CD86 blockade in context of RT improves cDC costimulatory status and CTL priming.
(A–D) Mice bearing 20 mm² TC-1 tumors received 0 Gy (n=6) or 20 Gy RT at day 0 in combination with either vehicle (PBS, n=8) or blocking mAb against CD80 (n=7) or CD86 (n=8) at day 0, 3 and 6. The cDC response was monitored by flow cytometry in the TdLN at day 8. **(A)** Absolute counts (#) of migratory cDCs1 and cDC2s. **(B)** Representative concatenated (n=6-8) flow cytometry plots depicting the percentage of CD80⁺ and/or PD-L1⁺ cells among migratory cDC1s and cDC2s in the TdLN per treatment group. Numbers indicate percentages. **(C,D)** Quantification of the populations represented in **(B)** among migratory cDC1s **(C)** and migratory cDC2s **(D)** from the TdLN. **(E–H)** The CD8⁺ T cell response was monitored by flow cytometry in the same experiment described in Figure 5. **(E,F)** Opt-SNE visualization of 1000 randomly selected CD44⁺ CD62L⁻ cells among CD8⁺ T cells per sample found in TdLNs at day 8 concatenated per treatment group. **(E)** Representative heat map of TCF-1 expression and **(F)** visualization of the TCF-1⁻ subpopulation in TdLN (encircled) in different treatment groups. **(G)** Frequency of CD44⁺TCF-1⁻ cells among CD8⁺ T cells found in the TdLN and among CD45⁺ cells in the tumor at day 8 post treatment. **(H)** Concatenated (n=11) contour plots depicting expression of the indicated markers on CD44⁺TCF-1⁻ cells and CD44⁺TCF-1⁺ cells within CD8⁺ T cells in the TdLN. Numbers indicate percentages. Data are from one experiment representative of two experiments. Error bars indicate SD. *P < 0.05, **P < 0.01, *** P < 0.001, **** P < 0.0001, ordinary one-way Anova with Dunnett's post hoc test in **A**, **C-E**. ns; not significant.

RT plus PD-1 blockade increases the Treg response, which is overruled by CD86 blockade, resulting in improved tumor control

PD-1 is the key target in cancer immunotherapy and its expression is considered a hallmark of suboptimally primed CTLs that lack full cytotoxic effector functions[62]. We found that $CD44^+TCF\text{-}1^-CD8^+$ T cells in the tumor after combined RT and CD86 blockade expressed PD-1, albeit to a lesser extent than $CD44^+TCF\text{-}1^+CD8^+$ T cells (**Supplementary Figure 8A**). In fact, both $Ki67^+$ CTLs and eTregs in the tumor expressed PD-1 (**Figure 7A**). PD-1 preferentially inhibits CD28 costimulation[31] and PD-1 blockade not only promotes Tconv responses[2] but also Treg responses by enabling TCR/CD28 signaling[63,64]. We therefore examined the effect of PD-1 blockade alone, or combined with CD86 blockade on RT-induced Treg and CTL responses. Strikingly, PD-1 blockade increased RT-induced eTreg priming and tumor infiltration (**Figure 7, B and C, Supplementary Figure 8, B and C**). This result argues that CD28 costimulation, enabled by PD-1 blockade, favors Treg priming in this tumor model, as does CTLA-4 blockade. Upon CD86 blockade, the RT-induced eTreg response was abrogated, both in absence or presence of PD-1 blockade (**Figure 7, B and C**). These data indicate that CD86 is required to engage CD28 on Tregs to drive their response. Importantly, following CD86 blockade, the frequency of proliferating ($Ki67^+$) $CD8^+$ T cells significantly increased in the tumor, while combined CD86 and PD-1 blockade increased this population in both TdLN and tumor (**Figure 7, B and D, Supplementary Figure 8, B and C**). These findings align with our initial observation that RT-induced Treg priming hampers the induction of a CTL response by RT.

We next assessed how inhibition of PD-1 and/or CD86 impacted RT-induced tumor control. PD-1 blockade alone failed to enhance RT-induced tumor regression and overall survival, in line with stimulation of the Treg response (**Figure 7, E and F, Supplementary Figure 8D**). CD86 blockade alone improved RT-induced tumor control from 48% to 62%, with a fraction of the tumors initially responding, but later relapsing. Combined PD-1 and CD86 blockade significantly increased overall survival compared to RT alone. The effect of CD86 blockade alone on overall mouse survival displayed a similar trend, but did not reach statistical significance. Taken together, in this lymphocyte-depleted tumor model, RT enhances eTreg priming while restraining tumor-reactive CTL priming, which is further enhanced by PD-1 blockade. This is likely because PD-1 blockade preferentially enables CD28 costimulation of Tregs (**Figure 7G**). CD86 blockade alone, or in combination with PD-1 blockade, counteracts eTreg priming through the inhibition of CD28 costimulation of Tregs. Inhibiting the Treg response facilitates tumor-reactive CTL priming and tumor control by RT upon CD86 blockade. With additional PD-1 blockade, $PD\text{-}1^+$ CTLs likely exhibit enhanced activity in the TME, explaining the improved tumor control.

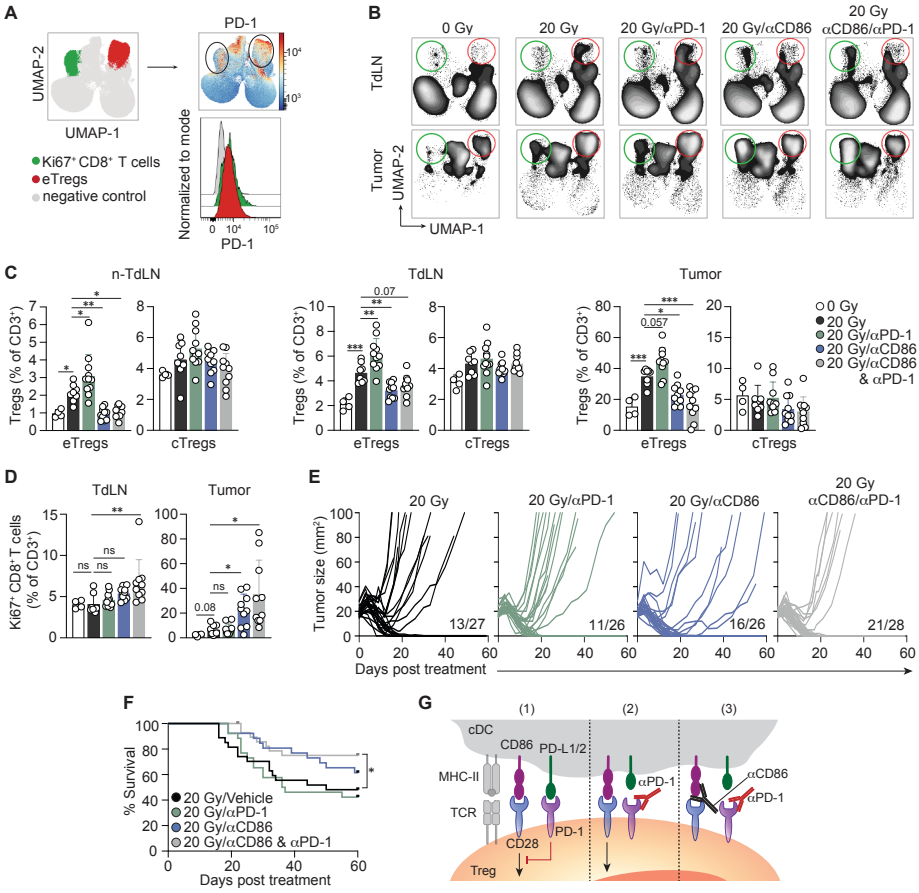

Figure 7. CD86-mediated CD28 costimulation is required for PD-1-dependent eTreg expansion.
(A) PD-1 expression on Ki67$^+$ CD8$^+$ T cells (green) and eTreg cells (red) in the tumor as identified in **Figure 5A,** presented as a heatmap and a representative histogram across all experimental conditions. **(B-D)** TC-1 tumor-bearing mice received 0 Gy (n=4) or 20 Gy RT on day 0 with vehicle (PBS, n=8) or blocking mAbs against PD-1 (n=11), CD86 (n=10), or the combination (n=10) on days 0, 3, and 6. CD3$^+$ lymphocyte responses were analyzed by flow cytometry in non-TdLN, TdLN and tumor on day 8. **(B)** UMAP visualization of treatment response of the CD3$^+$ subpopulations. Red circle indicates eTregs, and green circle Ki67$^+$ CD8$^+$ T cells (see **Supplementary Figure 8, B and C**). **(C)** Frequencies of eTregs and cTregs identified in Supplementary Figure 8B among CD3$^+$ cells in indicated tissues. **(D)** Quantification of the Ki67$^+$ CD8$^+$ T cell population among total CD3$^+$ cells in the TdLN and tumor (legend as in **C**). **(E)** Individual tumor growth curves and **(F)** overall survival of TC-1 tumor-bearing mice receiving RT on day 0 with vehicle (n=27), blocking mAbs against PD-1 (n=26), CD86 (n=26), or a combination (n=28) on days 0, 3, and 6. Proportion of mice that fully recovered is indicated. **(G)** Proposed effect of combined CD86 and PD-1 blockade on Tregs. (1) PD-L1/L2 on cDCs engages PD-1 that inhibits CD28 costimulation of Tregs. (2) PD-1 blockade enables CD28 costimulation of Tregs. (3) CD86 blockade inhibits CD28 costimulation of Tregs, which cannot be overruled by PD-1 blockade, impeding the Treg response. Data are from one experiment representative of two experiments. Error bars indicate SD. *P < 0.05, **P < 0.01, *** P < 0.001, ordinary one-way Anova with Dunnett's post hoc test in **C**; Brown-Forsythe Anova with Dunnett's T3 post hoc analysis in **D**; Mantel-Cox analysis in **F**. ns; no significance.

Discussion

The potential of RT to induce systemic T-cell responses to cancer has recently received much attention, but clinical evidence for abscopal, immune-mediated effects are scarce, even in combination with ICB[10]. We must therefore better understand the ability of RT to induce tumor-controlling T-cell responses, in the context of immunologically divergent cancer types. Comparison of *in vivo* tumor models of varying immunogenicity demonstrated that in immunogenic tumors, intra-tumoral $CD8^+$ T cells contributed to the RT response. In poorly immunogenic tumors, however, RT failed to elicit a systemic anti-tumor immune response and an abscopal effect[20]. We show that the TC-1 tumor model used in our study recapitulates lymphocyte-depleted human cancer types[3] that respond negatively to RT (**Figure 1A**). The TC-1 tumor expresses HPV-16 derived E6 and E7 antigens, but is not immunogenic and only regresses upon therapeutic vaccination[37]. We show that this tumor invites Tregs in the tumor and the TdLN, consistent with systemic immunosuppression clinically observed in this tumor type[65,66]. Priming tumor-specific CTLs in the TdLN depends on cDC1s that excel at tumor antigen cross-presentation[56,57]. The cDC2 subset favors $CD4^+$ T-cell priming, including Tconvs and Tregs[58,67]. In the TC-1 tumor, cDC2 frequency far exceeds cDC1 frequency (**Figure 2A**), which may favor Treg priming. Nevertheless, RT-induced TC-1 tumor regression is $CD8^+$ T-cell dependent. This finding suggests that in lymphocyte-depleted tumors, there is an unexploited, favorable CTL response that should be improved by the correct intervention(s).

Tregs serve to prevent or suppress unwanted Tconv responses against both self- and foreign antigens[68]. At steady state, "immature" or "tolerogenic" cDCs, that mainly express CD86 as costimulatory ligand[69], migrate from peripheral tissues to dLNs to present self-antigens and prevent responses of sporadic, autoreactive T cells. $FOXP3^+Helios^+$, thymus-derived cTregs exert this role at steady-state without clonal expansion or relocation to non-lymphoid tissues. Reportedly, the metabolic state of cDC2s may govern cTreg expansion, in part through CD86 upregulation[70]. Especially in tumors, limited nutrient resources and immunosuppressive factors may induce a metabolic state in cDCs that supports cTreg expansion[71]. Tregs help to control inflammation resulting from tissue injury, such as inflicted by RT. In this process, cTregs are recruited from dLNs to damaged tissues[72], where they present an eTreg phenotype[39]. The stimuli that drive the eTreg response are currently unknown. Murine and human tissue-resident eTregs have a conserved transcriptional signature that is most explicit in tumor-resident eTregs and contains a tissue-repair program[73]. In an irradiated tumor, next to extinguishing inflammation, these eTregs support extracellular matrix remodeling and tumor growth via their repair function[74] and may thereby impede RT efficacy.

We document that the TC-1 tumor at steady-state drives priming of Tregs in the TdLN that expand and populate the tumor. These cells co-express FOXP3 and Helios, indicating their tTreg identity. We find that the Treg response in the TC-1 tumor model is enforced by RT and further promoted by CTLA-4 blockade. Tregs constitutively express CTLA-4 that inhibits CD28 costimulation. Upon CTLA-4 blockade, both CD80 and CD86 are available to support the Treg response by CD28 costimulation[53]. However, we find that CD86 is the selective driver of this Treg response. This aligns with recent *in vitro* studies highlighting CD86 as the preferred ligand for CD28 costimulation of Tregs[75]. These authors attribute this preference to the constitutive presence of CTLA-4 on Tregs. Since CD86 exhibits lower affinity for CTLA-4 than CD80, Tregs predominantly rely on CD86 for CD28 costimulation[75]. We found that CD86 blockade, but not CD80 blockade, increased migratory cDC1 frequency in the TdLN and their combined CD80 and PD-L1 expression that favors the formation of a CD28-costimulatory CD80/PD-L1 heterodimer. These data suggest that Tregs in the TME constrain migratory and costimulatory properties of cDC1, thereby limiting CTL priming in the TdLN. Furthermore, as documented in other tumor settings[76], Treg accumulation in the TdLN can restrict CTL priming by inhibiting cDC1 activation.

In certain mouse tumor models (TSA and 4T1 breast cancer and MCA38 colon cancer), CTLA-4 blockade and RT have a combined therapeutic effect[23,38,49,50]. CTLA-4 likely promotes new T-cell priming in these models, given the increased TCR diversity of tumor-infiltrating T cells observed. Subsets of patients with metastatic non-small cell lung cancer[23] or metastatic melanoma[22] also displayed a combined effect of CTLA-4 blockade and RT. This was not the case in the TC-1 model, which we explain by increased Treg- over CTL priming. Efficacy of CTLA-4 blockade is known to largely rely on a high CTL- over Treg ratio in the tumor[77,78]. In T-cell devoid tumors, several factors work against a favorable CTL-to-Treg ratio, e.g. a higher cDC2-to-cDC1 ratio in the TME, limited RT-induced adjuvanticity[27] and/or RT-induced suppressive factors that prevent cDC1 maturation[79,80]. Reportedly, fractionated low dose RT is superior in eliciting IFN-I dependent optimization of cDC1 for CTL priming, because single high dose RT attenuates IFN-I release by promoting DNA degradation[38]. Consequently, 3x 8 Gy, but not 20 Gy, cooperated with CTLA-4 blockade to improve systemic anti-tumor immunity in TSA and 4T1 mouse models[23,38,49,50]. However, in our model, RT induced a strong Treg response to both 3x 8 Gy and 20 Gy and these schedules had no differential therapeutic effect. Thus, in Treg dominant tumors, CTLA-4 blockade may preferentially support Treg expansion[81] and not improve CTL-based tumor control, regardless of the RT regimen used[46,82].

In the TC-1 tumor setting, PD-1 blockade exacerbated the RT-induced eTreg response and consequently impeded the therapeutic CTL response. In agreement with this, PD-1 blockade was recently shown to promote Treg responses in certain cancer patients, potentially leading to cancer hyper-progression[63,83]. These studies showed that both Tregs and Tconvs can profit from CD28 costimulation that is enabled by PD-1 blockade[31]. In tumors that favor Treg- over CTL priming at steady state and display an exacerbated eTreg response upon RT, the conditions are met for further Treg priming and expansion upon PD-1 blockade. Our discovery that CD86 blockade abrogated the Treg response in this setting is therefore of potential clinical relevance. When CD86 was blocked, PD-1 blockade could not induce Treg expansion upon RT, indicating its dependence on CD86-mediated CD28 costimulation. Importantly, RT-induced CTL priming supported by CD86 blockade allowed for reversal of the Treg/CTL ratio, while PD-1 blockade likely improved CTL quality, enhancing tumor control. Our finding that CD86 blockade primarily inhibited the eTreg response is of interest, since it is advisable that ICB does not interfere with peripheral tolerance induction by cTregs to prevent adverse immune-related toxicities[84].

In conclusion, we reveal that in a model of lymphocyte-depleted cancer that favors myeloid and Treg infiltration, CTLA-4 and PD-1 blockade have the opposite effect on RT-induced tumor control than in immunogenic tumors with high Tconv infiltrates. This is due to exacerbation of RT-induced Treg responses that counteract the RT-induced CTL response. We therefore caution that CTLA-4 and/or PD-(L)1 blockade may likewise exacerbate RT-induced Treg responses in human lymphocyte-depleted cancer. Our findings argue that CD86 is a suitable target to inhibit undesired eTreg responses and a new candidate to improve Tconv responses to poorly immunogenic cancers, particularly in combination with RT. We acknowledge the limitation that our study is based on one murine tumor cell line representing lymphocyte-depleted cancer and that the immunological mechanisms revealed in our study should be corroborated in additional representative tumor models to validate the generality of our findings.

Methods

TCGA data analysis

Immune subtype classifications among 9126 tumors were collected from Thorsson et al.[3]. Patient-specific RT status and survival metrics were gathered from the UCSC Xena Platform using the *UCSCXenaTools* package[85] of which 7891 tumors had complete information available. Kaplan-Meier curves were generated for each immune subtype using overall survival (in months) by radiotherapy status (yes vs. no). For immune

subtype prediction, the C4/C5 subtypes were collapsed into a single immune subtype and tumors derived from the C3 and C4/C5 immune subtypes were selected (n=3939). Features derived from the CIBERSORT deconvolution algorithm and IFNg signature were subsequently used (n=23). Next, data was split into 70% and 30% training and testing datasets, respectively. The training data was scaled and centered before undergoing a 5-fold repeated cross-validation strategy to predict between C4/C5 vs. C3 using a K-nearest neighbor (KNN) model. The test data was then applied to evaluate model performance.

Murine microarray analysis

Microarray data and metadata was downloaded from *GSE85509* using *GEOquery.* Murine gene symbols were converted to human symbols using the *biomaRt* package. Immune cell types were deconvolved using *CIBERSORT* from the *immunedeconv* package and the IFNg signature was generated using the Ayers gene signature[86]. Next, the data from the TC-1 and MC38 cell lines were used as input into the trained KNN model for classification.

Tumor cells

The MC38 colon cancer cell line was purchased from Kerafast (Boston, MA) and TC-1 tumor cells (lung epithelial cells engineered to express HPV16 E6 and E7 proteins[34]) were obtained from Leiden University Medical Center in 2015 and the authors did not perform further authentication. MC38 and TC-1 cells were cultured in DMEM and RPMI 1640 (Gibco, Life Technologies) respectively, supplemented with 10% fetal calf serum (FCS), 0.1 mM non-essential amino acids, 1 mM sodium pyruvate, 2 mM L-glutamine, 10 mM HEPES and penicillin/streptomycin (Roche) at 37°C, 5% CO_2. MC38 and TC-1 cell stocks were tested negative for *Mycoplasma* by PCR, and thawed cells were used within 3 passages for *in vivo* experiments.

Tumor transplantation and RT

Six- to eight-week-old female C57BL/6Rj (B6) mice were purchased from Janvier Laboratories (Le Genest Saint Isle, France). At day -8, mice were anesthetized with isoflurane and injected subcutaneously (s.c) with either $1x10^6$ MC38 or $1x10^5$ TC-1 tumor cells in 50 µl HBSS. Tumor size was measured by calipers in two dimensions and calculated as: area (mm^2) = width x length. RT was initiated when the tumors reached 18-25 mm^2 (day 0) and mice were randomly assigned to different treatment groups. RT was applied using the SmART$^+$ system (Precision X-Ray, North Branford, CT). Mice were anesthetized with isoflurane and a cone-beam CT scan of the mice was performed. The tumor was localized on the CT scan and targeted with RT at 0.1 mm precision using round collimators 1.0 or 1.5 cm in diameter. A single fraction of 8 or 20

Gy (225 peak kilovoltage (kVp), filtered with 0.3 mm of copper (3 Gy/min)) was delivered. For fractionated dosage studies, a single dose of 8 Gy was delivered on days 0, 1 and 2. Control mice (indicated as 0 Gy) were anesthetized and received a cone-beam CT scan but were not exposed to RT. Mice were sacrificed when the tumor diameter reached 15 mm or when the tumor size reached >100 mm^2. In the survival curves, censored events indicate mice that were sacrificed due to treatment unrelated disease.

Therapeutic antibodies and reagents

Mice received intraperitoneal (i.p.) injections of depleting anti-CD8a-mAb (2.43, BioXCell) or anti-CD4-mAb (GK1.5, BioXCell) at 200 µg per mouse in 100 µl PBS starting at day -1 prior to RT (day 0) followed by days 3, 6 and 9. For Treg depletion experiments, mice were injected i.p. with 250 µg of depleting mouse IgG2a isotype CD25-mAb[48] (modified clone of PC61, Evitria) in 100 µl PBS at day -1 prior to RT and at day 5. Blocking mAbs to CTLA-4 (UC10-4F10-11, BioXCell), PD-1 (RMP1-14, BioXCell), CD80 (1G10, BioXCell) and CD86 (GL-1, BioXCell) were injected i.p. at either 100 µg (anti-CTLA-4 and anti-PD-1) or 200 µg (anti-CD80 and anti-CD86) per mouse in 100 µl PBS at the day of RT (day 0) and days 3, 6, and in case of anti-CTLA-4 also at day 9. Control mice were injected with equal amounts of PBS (vehicle) according to the treatment schedule indicated. FTY720 (Fingolimod; Cayman Chemical) was dissolved in 0.9% NaCl solution (vehicle) and administered at 2 mg/kg by oral gavage. FTY720 treatment started one day prior to RT and was repeated three times per week throughout the duration of the experiment.

Tissue preparation and flow cytometry

At the indicated time points, tumor-bearing mice were sacrificed, and the lymphoid tissues and tumors were isolated. Intra-tumoral injection of 5% Evans Blue dye (Sigma-Aldrich) in 50 ml PBS identified the axillary LN on the tumor bearing side as the TdLN, whereas the contralateral inguinal LN was defined as the non-TdLN. The TdLN was carefully kept out of the field of irradiation to prevent RT-induced attenuation of the adaptive immune responses in the LN[87]. Tumor tissue was mechanically disaggregated using a McIlwain tissue chopper (Mickle Laboratory Engineering), and a single-cell suspension was prepared by digesting the tissue in collagenase type A (Roche) and 25 µg/ml DNase I (Sigma) in serum-free DMEM for 45 min at 37°C. Enzyme activity was neutralized by adding medium with 10% FCS, and the tissue was dispersed by passing through a 70-µm cell strainer. To acquire single cell suspensions, LN tissue was punctured with a 27 G needle followed by incubation in 100 µg/mL Liberase™ TL (Roche) in serum-free DMEM for 30 min at 37°C. Enzyme activity was neutralized as described above and tissue was dispersed by passing through a 70-µm cell strainer. Peripheral blood cells were collected from tail blood of live mice in Microvette CB300

LH tubes (Sarstedt). Red blood cells were lysed in 0.14 M NH_4Cl and 0.017 M Tris-HCl (pH 7.2) for 1 min at room temperature. For surface staining, single cells of the isolated tissues (except blood samples) were first incubated with anti-CD16/32 (1:50, clone 2.4G2, BD Bioscience) supplemented with 10 µg/ml DNAse, to block unspecific Fc-receptor binding, for 10 min on ice. Next, surface antibody staining was performed (**Supplementary Table 1**) for 30 min in PBS containing 0.5% BSA and 0.01% sodium azide. For intracellular staining of transcription factors and cytokines, cells were fixed and permeabilized with the FOXP3 Transcription Factor Staining Buffer Set according to the manufacturer's protocol (Thermo Fischer Scientific). Dead cells were excluded by using Fixable Viability Near-infra red dye (1:1000, Life Technologies), Zombie Red Fixable Viability Kit (1:5000, BioLegend) or Zombie UV fixable viability Kit (1:500, BioLegend). Cytokine detection in tumor and lymph node single cell preparations was performed following ex vivo stimulation in presence of 1 µg/ml GolgiPlug (BD Biosciences) with 50 ng/ml phorbol 12-myristate 13-acetate (PMA, Sigma Aldrich) and 1 µM ionomycin (Sigma Aldrich) dissolved in DMSO and diluted in 100 µl IMDM containing 8% FCS for 3 h at 37°C, 5% CO_2. Control (unstimulated) cells were treated with an equal volume of DMSO in presence of GolgiPlug diluted in IMDM with 8% FCS. Absolute cell numbers were determined by adding AccuCount Blank Particles (7-7.9 µm, Spherotech) to each sample, prior to flow cytometry analysis. Fluorescence minus one (FMO) was used as a negative control for activation markers. Flow cytometry was performed using a BD FACSymphony™ A5 SORP flow cytometer or the 5-laser Cytek Aurora. All generated data was analyzed using FlowJo and OMIQ software (Dotmatics, Boston, MA).

Data analysis

Dimensionality reduction and FlowSOM[88] analysis of flow cytometry data was performed using OMIQ software. Following conventional marker expression analysis, the population of interest was manually gated, and down-sampling was performed to select the maximal number of cells per tissue representative for all tissue types included, as indicated in the figure legends. Tumor samples containing <600 cells of the subsampled population were excluded from analysis (see **Figure 5D**). K-means clustering of the indicated populations was performed using FlowSOM, including all markers indicated, except for live/dead and CD45 and in case of the $CD8^+$ T-cell population (see **Figure 6, E and F**) also without CD3. Dimension reduction and visualization was performed using uniform manifold approximation and projection (UMAP) analysis[89] and opt-SNE analysis[90], including the same markers as described above and by using the default OMIQ settings.

Statistical analysis

All statistical data were analyzed using GraphPad Prism version 9 (GraphPad Software, La Jolla, CA). Statistical analyses were performed as indicated in the figure legends. Ordinary one-way Anova was performed in case sample sizes were n>8, more than three experimental groups were compared and if the assumption for normal distribution was met. In case sample sizes were n<8 and if normal distribution could not be assumed, Kruskal-Wallis analysis was applied. A P value <0.05 was considered statistically significant; *p<0.05, **p<0.01, ***p<0.001, ****p<0.0001. Data are presented as mean + S.D.

Study approval

Mice were maintained in individually ventilated cages (Innovive, San Diego, CA) under specific pathogen-free conditions. Only female mice were used to facilitate randomization of the large treatment groups. All mouse experiments were performed in accordance with institutional and national guidelines under license number AVD3010020173106 of the Central Committee Animal Experiments (Centrale Commissie Dierproeven) and were approved by the Animal Welfare Body (IVD) of the Netherlands Cancer Institute.

Data availability

Data is available upon request. Values for all data points found in graphs can be found in file with supporting data values.

Author contributions

Conception and design: E.F., J. Bo.
Development of methodology: E.F., T.W.B., I.V.
Experimental advice: D.M.T.B., T.W.B., J. Bu., M.D.S., I.V.
Acquisition of data: E.F., D.M.T.B., T.W.B., J. Bu., M.D.S.
Analysis and interpretation of data: E.F., T.W.B. , J. Bo.
Writing of manuscript: E.F., J.Bo.
Critical reading and editing of the paper: D.M.T.B., T.W.B., J. Bu., M.D.S., I.V.

Acknowledgements

We thank dr. Ramon Arens for providing the CD80 and CD86 blocking antibodies, and dr. Sergio Quezada for providing the CD25 IgG2a *in vivo* depletion antibody. We thank all members of the Immunology department at LUMC, and all members of the Tumor Biology & Immunology department at NKI, for their insightful input and helpful discussions. We thank the flow cytometry facility, animal laboratory facility and the intervention unit of the Netherlands Cancer Institute for technical assistance. This work was supported by Dutch Cancer Society Grant NKI 2017-10894 to I. Verbrugge and J. Borst, Dutch Cancer Society Grant NKI 2017-11079 to J. Borst and a grant from the Oncode Institute to J. Borst.

References

1. Haslam, A. & Prasad, V. Estimation of the Percentage of US Patients With Cancer Who Are Eligible for and Respond to Checkpoint Inhibitor Immunotherapy Drugs. *JAMA Netw Open* 2, (2019).

2. Huang, A. C. *et al.* T-cell invigoration to tumour burden ratio associated with anti-PD-1 response. *Nature* 545, 60–65 (2017).

3. Thorsson, V. *et al.* The Immune Landscape of Cancer. *Immunity* 48, 812-830.e14 (2018).

4. Luca, B. A. *et al.* Atlas of clinically distinct cell states and ecosystems across human solid tumors. *Cell* 184, 5482-5496.e28 (2021).

5. Combes, A. J. *et al.* Discovering dominant tumor immune archetypes in a pan-cancer census. *Cell* 185, 184-203.e19 (2022).

6. Hiam-Galvez, K. J., Allen, B. M. & Spitzer, M. H. Systemic immunity in cancer. *Nat Rev Cancer* 21, 345–359 (2021).

7. Gajewski, T. F. The Next Hurdle in Cancer Immunotherapy: Overcoming the Non-T-Cell-Inflamed Tumor Microenvironment. *Semin Oncol* 42, 663–671 (2015).

8. Wellenstein, M. D. & de Visser, K. E. Cancer-Cell-Intrinsic Mechanisms Shaping the Tumor Immune Landscape. *Immunity* 48, 399–416 (2018).

9. Chen, D. S. & Mellman, I. Elements of cancer immunity and the cancer-immune set point. *Nature* 541, 321–330 (2017).

10. Pointer, K. B., Pitroda, S. P. & Weichselbaum, R. R. Radiotherapy and immunotherapy: open questions and future strategies. *Trends Cancer* 8, 9–20 (2022).

11. Kroon, P. *et al.* Radiotherapy and Cisplatin Increase Immunotherapy Efficacy by Enabling Local and Systemic Intratumoral T-cell Activity. *Cancer Immunol Res* 7, 670–682 (2019).

12. Lee, Y. *et al.* Therapeutic effects of ablative radiation on local tumor require CD8+ T cells: changing strategies for cancer treatment. *Blood* 114, 589–595 (2009).

13. Takeshima, T. *et al.* Local radiation therapy inhibits tumor growth through the generation of tumor-specific CTL: its potentiation by combination with Th1 cell therapy. *Cancer Res* 70, 2697–2706 (2010).

14. Lugade, A. A. *et al.* Local radiation therapy of B16 melanoma tumors increases the generation of tumor antigen-specific effector cells that traffic to the tumor. *J Immunol* 174, 7516–7523 (2005).

15. Golden, E. B. & Apetoh, L. Radiotherapy and immunogenic cell death. *Semin Radiat Oncol* 25, 11–17 (2015).

16. Böttcher, J. P. & Reis e Sousa, C. The Role of Type 1 Conventional Dendritic Cells in Cancer Immunity. *Trends Cancer* 4, 784–792 (2018).

17. Abuodeh, Y., Venkat, P. & Kim, S. Systematic review of case reports on the abscopal effect. *Curr Probl Cancer* 40, 25–37 (2016).

18. Demaria, S. *et al.* Ionizing radiation inhibition of distant untreated tumors (abscopal effect) is immune mediated. *Int J Radiat Oncol Biol Phys* 58, 862–870 (2004).

19. Buchwald, Z. S. *et al.* Tumor-draining lymph node is important for a robust abscopal effect stimulated by radiotherapy. *J Immunother Cancer* 8, (2020).

20. Lai, J. Z. *et al.* Abscopal Effects of Local Radiotherapy Are Dependent on Tumor Immunogenicity. *Front Oncol* 11, (2021).

21. Voorwerk, L. *et al.* Immune induction strategies in metastatic triple-negative breast cancer to enhance the sensitivity to PD-1 blockade: the TONIC trial. *Nat Med* 25, 920–928 (2019).

22. Twyman-Saint Victor, C. *et al.* Radiation and dual checkpoint blockade activate non-redundant immune mechanisms in cancer. *Nature* 520, 373–377 (2015).

23. Formenti, S. C. *et al.* Radiotherapy induces responses of lung cancer to CTLA-4 blockade. *Nat Med* 24, 1845–1851 (2018).

24. Theelen, W. S. M. E. *et al.* Effect of Pembrolizumab After Stereotactic Body Radiotherapy vs Pembrolizumab Alone on Tumor Response in Patients With Advanced Non-Small Cell Lung Cancer: Results of the PEMBRO-RT Phase 2 Randomized Clinical Trial. *JAMA Oncol* 5, 1276–1282 (2019).

25. Arina, A. *et al.* Tumor-reprogrammed resident T cells resist radiation to control tumors. *Nat Commun* 10, (2019).

26. Crittenden, M. R. *et al.* Tumor cure by radiation therapy and checkpoint inhibitors depends on pre-existing immunity. *Sci Rep* 8, (2018).

27. Blair, T. C. *et al.* Fluorescent tracking identifies key migratory dendritic cells in the lymph node after radiotherapy. *Life Sci Alliance* 5, (2022).

28. Mondini, M. *et al.* CCR2-Dependent Recruitment of Tregs and Monocytes Following Radiotherapy Is Associated with TNFα-Mediated Resistance. *Cancer Immunol Res* 7, 376–387 (2019).

29. Esensten, J. H., Helou, Y. A., Chopra, G., Weiss, A. & Bluestone, J. A. CD28 Costimulation: From Mechanism to Therapy. *Immunity* 44, 973–988 (2016).

30. Wing, K. *et al.* CTLA-4 control over Foxp3+ regulatory T cell function. *Science* 322, 271–275 (2008).

31. Hui, E. *et al.* T cell costimulatory receptor CD28 is a primary target for PD-1-mediated inhibition. *Science* 355, 1428–1433 (2017).

32. Mosely, S. I. S. *et al.* Rational Selection of Syngeneic Preclinical Tumor Models for Immunotherapeutic Drug Discovery. *Cancer Immunol Res* 5, 29–41 (2017).

33. Hos, B. J. *et al.* Identification of a neo-epitope dominating endogenous CD8 T cell responses to MC-38 colorectal cancer. *Oncoimmunology* 9, (2019).

34. Lin, K. Y. *et al.* Treatment of established tumors with a novel vaccine that enhances major histocompatibility class II presentation of tumor antigen. *Cancer Res* 56, (1996).

35. Ahrends, T. *et al.* CD4+ T Cell Help Confers a Cytotoxic T Cell Effector Program Including Coinhibitory Receptor Downregulation and Increased Tissue Invasiveness. *Immunity* 47, 848-861.e5 (2017).

36. Perez-Ruiz, E. *et al.* Prophylactic TNF blockade uncouples efficacy and toxicity in dual CTLA-4 and PD-1 immunotherapy. *Nature* 569, 428–432 (2019).

37. Ahrends, T. *et al.* CD27 Agonism Plus PD-1 Blockade Recapitulates CD4+ T-cell Help in Therapeutic Anticancer Vaccination. *Cancer Res* 76, 2921–2931 (2016).

38. Vanpouille-Box, C. *et al.* DNA exonuclease Trex1 regulates radiotherapy-induced tumour immunogenicity. *Nat Commun* 8, 15618 (2017).

39. Smigiel, K. S. *et al.* CCR7 provides localized access to IL-2 and defines homeostatically distinct regulatory T cell subsets. *J Exp Med* 211, 121–136 (2014).

40. Thornton, A. M. *et al.* Expression of Helios, an Ikaros transcription factor family member, differentiates thymic-derived from peripherally induced Foxp3+ T regulatory cells. *J Immunol* 184, 3433–3441 (2010).

41. Bauer, C. A. *et al.* Dynamic Treg interactions with intratumoral APCs promote local CTL dysfunction. *J Clin Invest* 124, 2425–2440 (2014).

42. Matloubian, M. *et al.* Lymphocyte egress from thymus and peripheral lymphoid organs is dependent on S1P receptor 1. *Nature* 427, 355–360 (2004).

43. Chen, Z. *et al.* TCF-1-Centered Transcriptional Network Drives an Effector versus Exhausted CD8 T Cell-Fate Decision. *Immunity* 51, 840-855.e5 (2019).

44. Zhao, X., Shan, Q. & Xue, H. H. TCF1 in T cell immunity: a broadened frontier. *Nat Rev Immunol* 22, 147–157 (2022).

45. Muroyama, Y. *et al.* Stereotactic Radiotherapy Increases Functionally Suppressive Regulatory T Cells in the Tumor Microenvironment. *Cancer Immunol Res* 5, 992–1004 (2017).

46. Ji, D. *et al.* Combination of radiotherapy and suppression of Tregs enhances abscopal antitumor effect and inhibits metastasis in rectal cancer. *J Immunother Cancer* 8, (2020).

47. Sainz-Perez, A., Lim, A., Lemercier, B. & Leclerc, C. The T-cell receptor repertoire of tumor-infiltrating regulatory T lymphocytes is skewed toward public sequences. *Cancer Res* 72, 3557–3569 (2012).

48. Arce Vargas, F. *et al.* Fc-Optimized Anti-CD25 Depletes Tumor-Infiltrating Regulatory T Cells and Synergizes with PD-1 Blockade to Eradicate Established Tumors. *Immunity* 46, 577–586 (2017).

49. Dewan, M. Z. *et al.* Fractionated but not single-dose radiotherapy induces an immune-mediated abscopal effect when combined with anti-CTLA-4 antibody. *Clin Cancer Res* 15, 5379–5388 (2009).

50. Rudqvist, N. P. *et al.* Radiotherapy and CTLA-4 Blockade Shape the TCR Repertoire of Tumor-Infiltrating T Cells. *Cancer Immunol Res* 6, 139–150 (2018).

51. Postow, M. A. *et al.* Immunologic correlates of the abscopal effect in a patient with melanoma. *N Engl J Med* 366, 925–931 (2012).

52. Simpson, T. R. *et al.* Fc-dependent depletion of tumor-infiltrating regulatory T cells co-defines the efficacy of anti-CTLA-4 therapy against melanoma. *J Exp Med* 210, 1695–1710 (2013).

53. Marangoni, F. *et al.* Expansion of tumor-associated Treg cells upon disruption of a CTLA-4-dependent feedback loop. *Cell* 184, 3998-4015.e19 (2021).

54. Salomon, B. *et al.* B7/CD28 costimulation is essential for the homeostasis of the CD4+CD25+ immunoregulatory T cells that control autoimmune diabetes. *Immunity* 12, 431–440 (2000).

55. Marangoni, F. *et al.* Tumor Tolerance-Promoting Function of Regulatory T Cells Is Optimized by CD28, but Strictly Dependent on Calcineurin. *J Immunol* 200, 3647–3661 (2018).

56. Broz, M. L. *et al.* Dissecting the tumor myeloid compartment reveals rare activating antigen-presenting cells critical for T cell immunity. *Cancer Cell* 26, 638–652 (2014).

57. Salmon, H. *et al.* Expansion and Activation of CD103(+) Dendritic Cell Progenitors at the Tumor Site Enhances Tumor Responses to Therapeutic PD-L1 and BRAF Inhibition. *Immunity* 44, 924–938 (2016).

58. Binnewies, M. *et al.* Unleashing Type-2 Dendritic Cells to Drive Protective Antitumor CD4+ T Cell Immunity. *Cell* 177, 556-571.e16 (2019).

59. Sugiura, D. *et al.* Restriction of PD-1 function by cis-PD-L1/CD80 interactions is required for optimal T cell responses. *Science* 364, 558–566 (2019).

60. Zhao, Y. *et al.* PD-L1:CD80 Cis-Heterodimer Triggers the Co-stimulatory Receptor CD28 While Repressing the Inhibitory PD-1 and CTLA-4 Pathways. *Immunity* 51, 1059-1073.e9 (2019).

61. Oh, S. A. *et al.* PD-L1 expression by dendritic cells is a key regulator of T-cell immunity in cancer. *Nat Cancer* 1, 681–691 (2020).

62. Philip, M. & Schietinger, A. CD8+ T cell differentiation and dysfunction in cancer. *Nat Rev Immunol* 22, 209–223 (2022).

63. Kumagai, S. *et al.* The PD-1 expression balance between effector and regulatory T cells predicts the clinical efficacy of PD-1 blockade therapies. *Nat Immunol* 21, 1346–1358 (2020).

64. Tan, C. L. *et al.* PD-1 restraint of regulatory T cell suppressive activity is critical for immune tolerance. *J Exp Med* 218, (2021).

65. Deng, L. *et al.* Accumulation of foxp3+ T regulatory cells in draining lymph nodes correlates with disease progression and immune suppression in colorectal cancer patients. *Clin Cancer Res* 16, 4105–4112 (2010).

66. Wang, L. *et al.* Connecting blood and intratumoral Treg cell activity in predicting future relapse in breast cancer. *Nat Immunol* 20, 1220–1230 (2019).

67. Gerner, M. Y., Casey, K. A., Kastenmuller, W. & Germain, R. N. Dendritic cell and antigen dispersal landscapes regulate T cell immunity. *J Exp Med* 214, 3105–3122 (2017).

68. Vignali, D. A. A., Collison, L. W. & Workman, C. J. How regulatory T cells work. *Nat Rev Immunol* 8, 523–532 (2008).

69. Lutz, M. B. & Schuler, G. Immature, semi-mature and fully mature dendritic cells: Which signals induce tolerance or immunity? *Trends Immunol* 23, 445–449 (2002).

70. Pelgrom, L. R. *et al.* LKB1 expressed in dendritic cells governs the development and expansion of thymus-derived regulatory T cells. *Cell Res* 29, 406–419 (2019).

71. Møller, S. H., Wang, L. & Ho, P. C. Metabolic programming in dendritic cells tailors immune responses and homeostasis. *Cell Mol Immunol* 19, 370–383 (2022).

72. Li, J., Tan, J., Martino, M. M. & Lui, K. O. Regulatory T-Cells: Potential Regulator of Tissue Repair and Regeneration. *Front Immunol* 9, (2018).

73. Delacher, M. *et al.* Single-cell chromatin accessibility landscape identifies tissue repair program in human regulatory T cells. *Immunity* 54, 702-720.e17 (2021).

74. Wirsdörfer, F. & Jendrossek, V. The Role of Lymphocytes in Radiotherapy-Induced Adverse Late Effects in the Lung. *Front Immunol* 7, (2016).

75. Halliday, N. *et al.* CD86 Is a Selective CD28 Ligand Supporting FoxP3+ Regulatory T Cell Homeostasis in the Presence of High Levels of CTLA-4. *Front Immunol* 11, (2020).

76. Zagorulya, M. *et al.* Tissue-specific abundance of interferon-gamma drives regulatory T cells to restrain DC1-mediated priming of cytotoxic T cells against lung cancer. *Immunity* 56, 386-405.e10 (2023).

77. Liakou, C. I. *et al.* CTLA-4 blockade increases IFNgamma-producing CD4+ICOShi cells to shift the ratio of effector to regulatory T cells in cancer patients. *Proc Natl Acad Sci U S A* 105, 14987–14992 (2008).

78. Quezada, S. A., Peggs, K. S., Curran, M. A. & Allison, J. P. CTLA4 blockade and GM-CSF combination immunotherapy alters the intratumor balance of effector and regulatory T cells. *J Clin Invest* 116, 1935–1945 (2006).

79. Wennerberg, E. *et al.* CD73 Blockade Promotes Dendritic Cell Infiltration of Irradiated Tumors and Tumor Rejection. *Cancer Immunol Res* 8, 465–478 (2020).

80. Hsieh, R. C. E. *et al.* ATR-mediated CD47 and PD-L1 up-regulation restricts radiotherapy-induced immune priming and abscopal responses in colorectal cancer. *Sci Immunol* 7, (2022).

81. Kavanagh, B. *et al.* CTLA4 blockade expands FoxP3+ regulatory and activated effector CD4+ T cells in a dose-dependent fashion. *Blood* 112, 1175–1183 (2008).

82. Balázs, K. *et al.* Radiotherapy-Induced Changes in the Systemic Immune and Inflammation Parameters of Head and Neck Cancer Patients. *Cancers (Basel)* 11, (2019).

83. Kamada, T. *et al.* PD-1+ regulatory T cells amplified by PD-1 blockade promote hyperprogression of cancer. *Proc Natl Acad Sci U S A* 116, 9999–10008 (2019).

84. Martins, F. *et al.* Adverse effects of immune-checkpoint inhibitors: epidemiology, management and surveillance. *Nat Rev Clin Oncol* 16, 563–580 (2019).

85. Goldman, M. *et al.* The UCSC Xena platform for public and private cancer genomics data visualization and interpretation. *bioRxiv* 326470 (2019) doi:10.1101/326470.

86. Ayers, M. *et al.* IFN-γ-related mRNA profile predicts clinical response to PD-1 blockade. *J Clin Invest* 127, 2930–2940 (2017).

87. Marciscano, A. E. *et al.* Elective Nodal Irradiation Attenuates the Combinatorial Efficacy of Stereotactic Radiation Therapy and Immunotherapy. *Clin Cancer Res* 24, 5058–5071 (2018).

88. Van Gassen, S. *et al.* FlowSOM: Using self-organizing maps for visualization and interpretation of cytometry data. *Cytometry A* 87, 636–645 (2015).

89. Becht, E. *et al.* Dimensionality reduction for visualizing single-cell data using UMAP. *Nat Biotechnol* 37, 38–47 (2018).

90. Belkina, A. C. *et al.* Automated optimized parameters for T-distributed stochastic neighbor embedding improve visualization and analysis of large datasets. *Nat Commun* 10, (2019).

Supplementary Information

Supplementary Figures

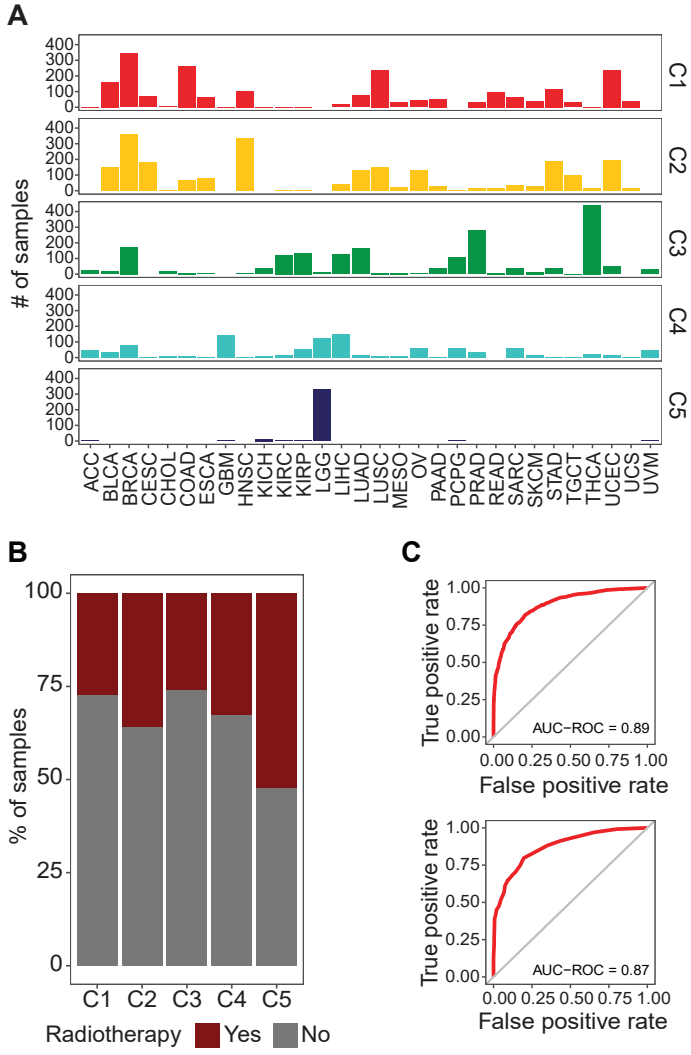

Supplementary Figure 1- Related to Figure 1 (A – B).
(A) Distribution of TCGA tumors (for tumor type abbreviation, see Supplementary Table 2) over the immune subtypes for which RT treatment (yes or no) was known. Bar heights indicate number of samples per tumor type. The total number of samples per tumor immune subtype (C1-C5) is indicated in **Figure 1A**. **(B)** Distribution of samples that received RT (red) or not (grey) for each tumor immune subtype. **(C)** Training (upper panel) and testing (lower panel) receiver operating curves (ROC) and area under the curve (AUC) calculation of a k-nearest neighbor's model training to classify C3 vs. C4/C5 TCGA immune subtypes. Training and testing were split 75% and 25%, respectively.

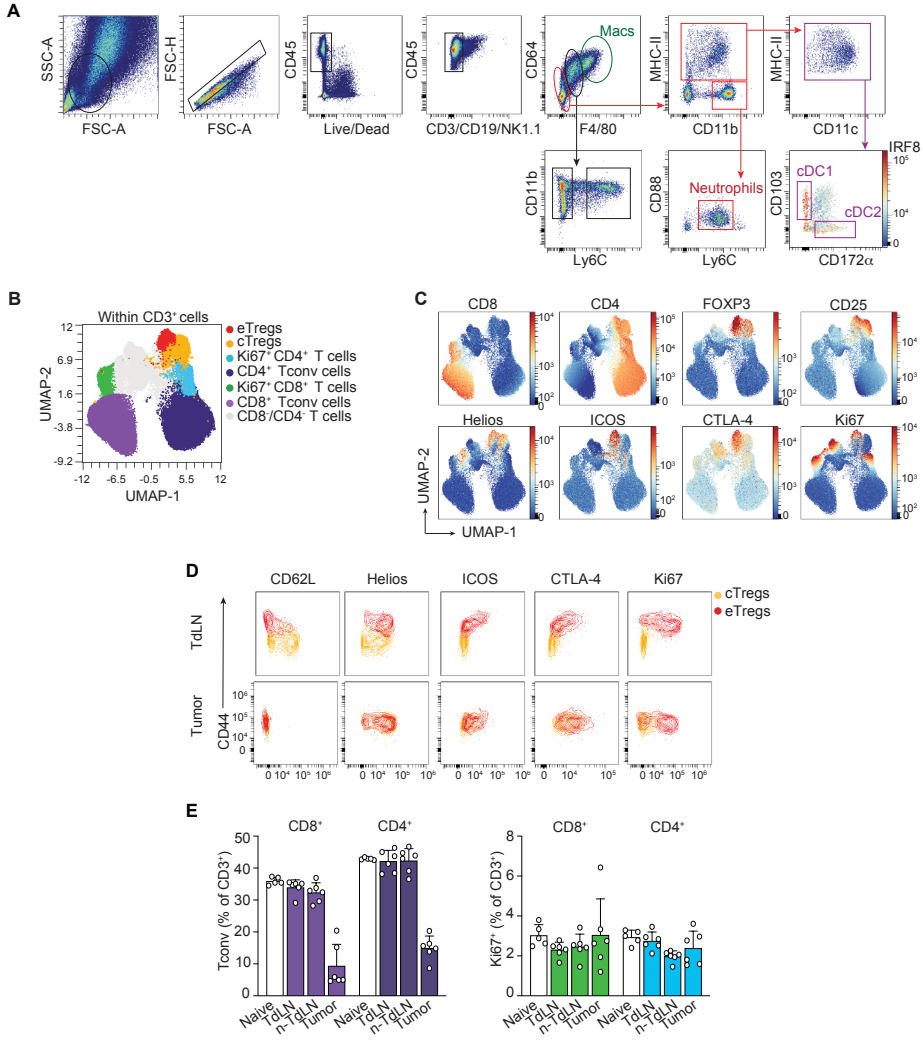

Supplementary Figure 2 - Related to Figure 2 (A – E).
(A) Representative gating strategy of the myeloid populations found in 50 mm^2 TC-1 tumors. **(B-C)** UMAP display of 5000 randomly selected CD3$^+$ cells per sample found in non-TdLN, TdLN and tumors at day 8 of all treatment groups combined. FlowSOM guided clustering **(B)** identifying the CD3$^+$ cell populations and **(C)** representative heat map visualization of the markers that identify the CD3$^+$ (T-cell) subpopulations. **(D)** Representative flow cytometry plots overlaying the in **(E)** identified cTreg and eTreg populations for TdLN (upper row) and tumor (lower row). **(E)** Percentage of the in **(B)** identified CD8$^+$ and CD4$^+$ Tconv populations (left) and Ki67$^+$CD8$^+$ and Ki67$^+$CD4$^+$ Tconv populations (right) among CD3$^+$ cells in the indicated tissues. Error bars indicate SD. Data is from one experiment, representative of two experiments.

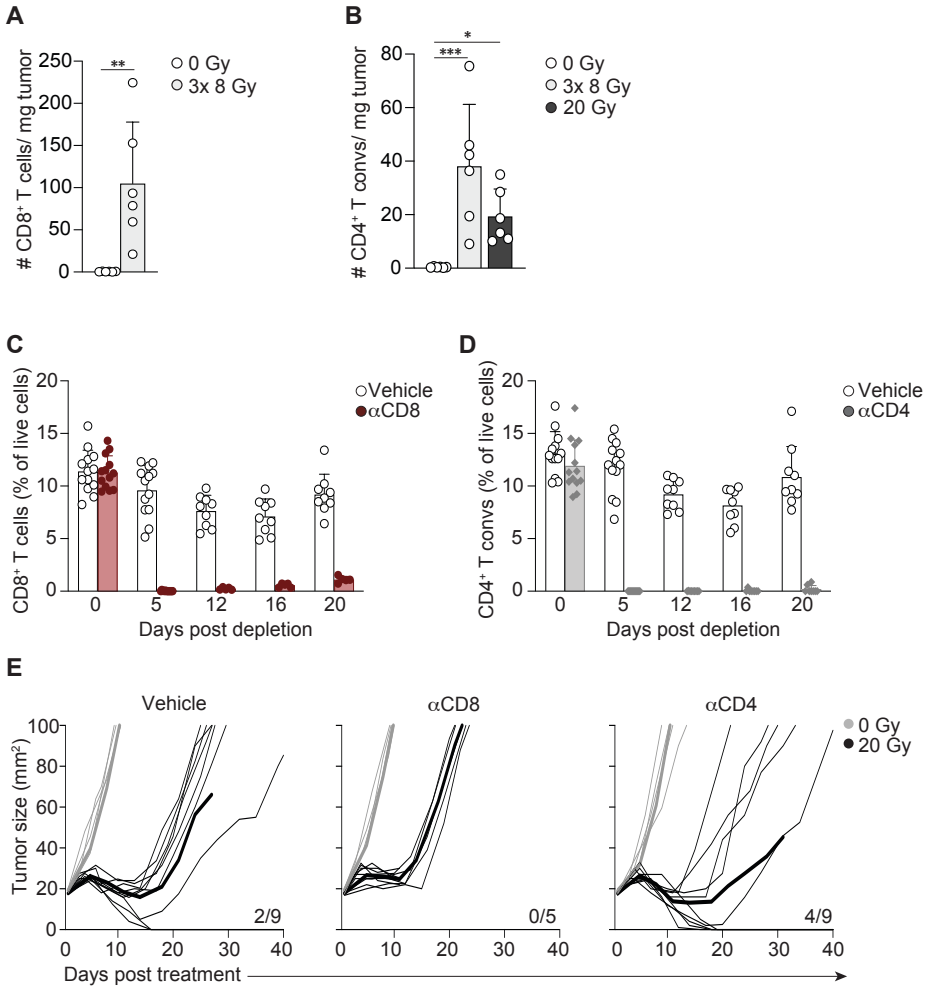

Supplementary Figure 3 – Related to Figure 2 (F - H).
(A) Absolute number (#) of total CD8⁺ T cells in TC-1 tumors treated with 8 Gy on three consecutive days (3x 8 Gy, n=6) or control (0 Gy, n=6) at day 8 post-RT. **(B)** Absolute number of (FOXP3⁻) CD4⁺ Tconv cells in TC-1 tumors treated with either 3x 8 Gy (n=6), 20 Gy (n=6) or control (0 Gy, n=6). **(C,D)** TC-1 tumor bearing mice were treated with 20 Gy RT (n=9/group) or control (0 Gy, n=4/group) at day 0 in combination with vehicle (PBS) or depleting mAbs against CD8 or CD4. **(C)** Frequency of CD8⁺ (left) or CD4⁺ Tconvs (right) among live cells in blood over time. The 0 Gy control group and 20 Gy groups are combined (Vehicle (PBS), n=13; aCD8, n=13; aCD4, n=13). **(E)** Individual tumor outgrowth curves belonging to **Figure 2H**. Thick lines indicate group averages. Data is from one experiment, representative of two experiments. Error bars indicate SD. *P < 0.05, **P < 0.01, *** P < 0.001, Mann-Whitney test in **A** and **B**. ns; not significant.

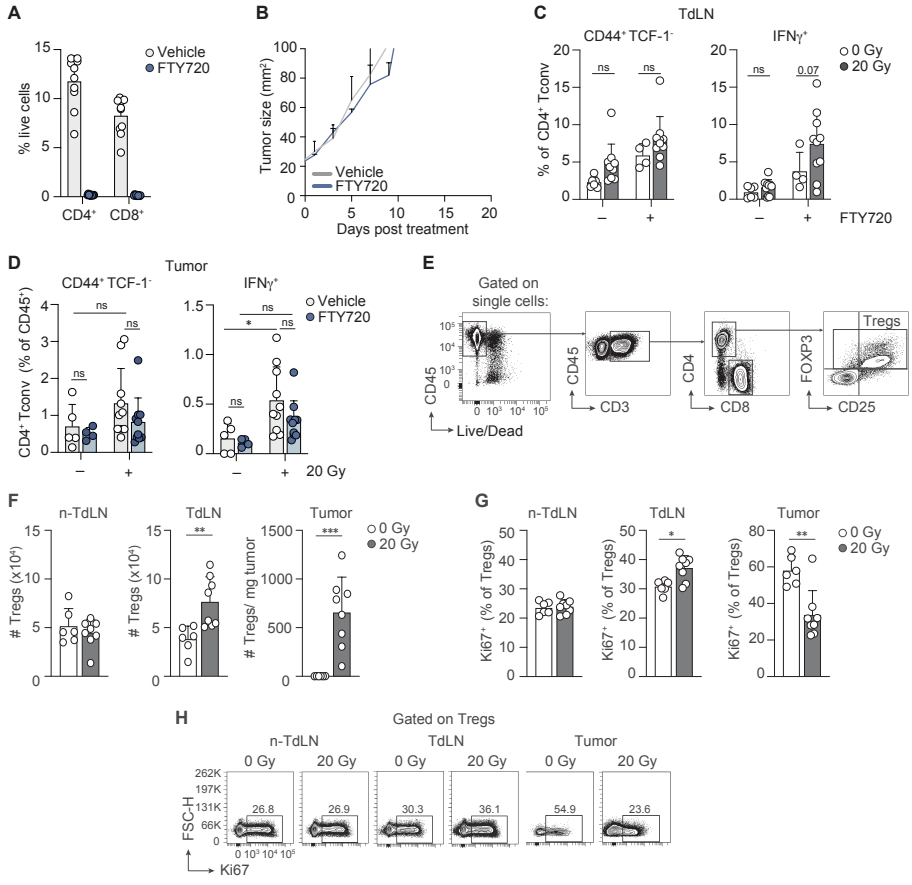

Supplementary Figure 4 – Related to Figure 3 (A – H).
(A-D) Data is from the same experiment described in **Figure 3, A-D**. TC-1 tumor bearing mice received 20 Gy RT (n=10/group) or 0 Gy (n=4-6/group) when tumor sizes reached ~20 mm² (day 0) in combination with FTY720 or vehicle (NaCl) by oral gavage, starting at day -1 and followed by days 3 and 5. At day 8, the TdLN and tumor were isolated and the (FOXP3⁻) CD4⁺ T cell response was analyzed. **(A,B)** Frequency of CD4⁺ and CD8⁺ Tconvs among live cells in blood at day 7 **(A)** and average tumor outgrowth curves **(B)** in TC-1 tumor bearing mice treated with 0 Gy and FTY720 or vehicle. **(C,D)** Frequency of CD44⁺TCF-1⁻ and IFNγ⁺ cells among CD4⁺ T cells in the TdLN **(C)** and in the tumor **(D)** of mice treated with 0 Gy or 20 Gy.**(E-G)** Monitoring of the (FOXP3⁺CD25⁺) Treg response to 20 Gy RT (n=8) or 0 Gy (n=6) in TC-1 tumor bearing mice by flow cytometry at day 8 post treatment. **(E)** Representative gating strategy of Treg cells, based on FOXP3⁺ and CD25⁺ expression. **(F)** Absolute counts (#) of total Treg cells in the non-TdLN, TdLN and tumor. **(G)** Percentage of Ki67⁺ cells among Tregs in the indicated tissues. **(H)** Representative concatenated (0 Gy, n=6; 20 Gy, n=8) flow cytometry plots depicting Ki67⁺ cells among Treg cells found in the non-TdLN, TdLN and tumor at day 8 post treatment. Numbers indicate the percentage of Ki67⁺ cells. Data is from one experiment, representative of two experiments. Error bars indicate SD. *P < 0.05, **P < 0.01, *** P < 0.001, two-way Anova with Tukey's post hoc test in **C** and **D**, Mann-Whitney test in **F** and **G**. ns; not significant.

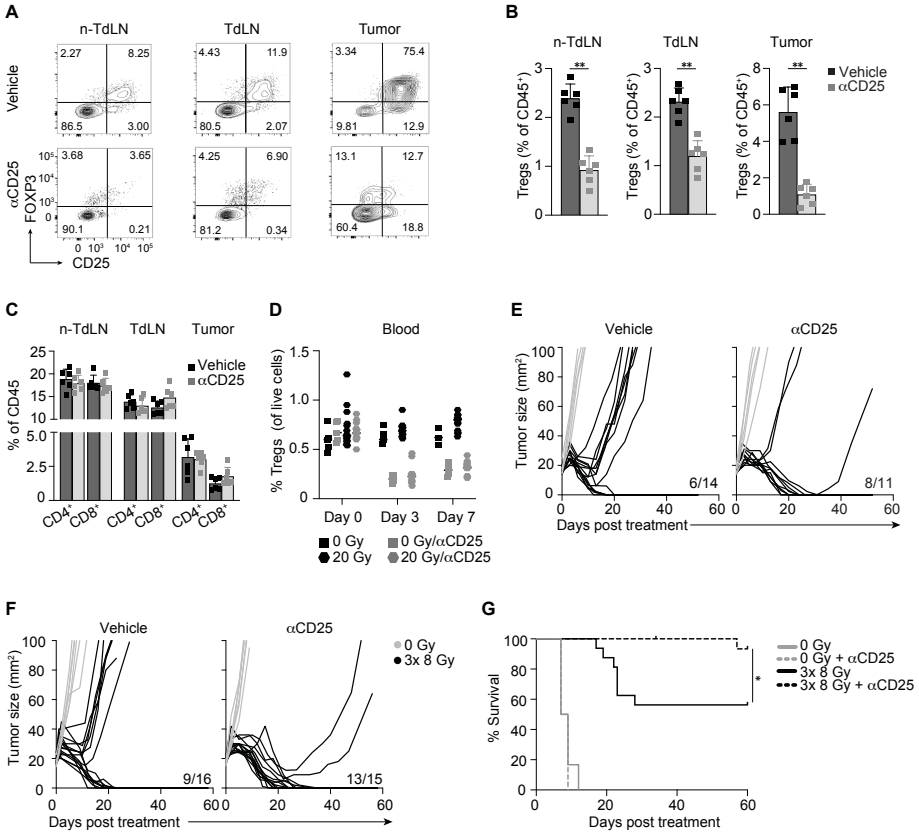

Supplementary Figure 5 - Related to Figure 3(I).
(A-C) TC-1 tumor bearing mice were treated i.p. with a depleting mAb against CD25 (n=6) or vehicle (PBS, n=6) when tumor size reached ~20 mm^2 (day 0). At day 4, the non-TdLN, TdLN and tumor were harvested and the Treg response was analyzed by flow cytometry. **(A)** Representative flow cytometry plots and **(B)** quantification depicting the frequency of total Tregs in the indicated tissues. **(C)** Proportion of CD4$^+$ and CD8$^+$ Tconvs among CD45$^+$ cells found in the indicated tissues following treatment. **(D)** Frequency of total Tregs among live cells measured in blood over time in the indicated treatment groups and **(E)** the individual tumor growth curves of the data described in **Figure 3I**. **(F)** Individual tumor growth curves and **(G)** overall survival of TC-1 tumor bearing mice treated with 0 Gy (n=6) or 3x8 Gy (n =15-16) in combination with a depleting mAb against CD25 or vehicle (PBS) at day -1 and 5 post RT. Ratios indicate the number of mice that showed full recovery upon treatment. Data are from one experiment representative of two experiments. Error bars indicate SD. *P < 0.05, **P < 0.01, Mann-Whitney test in **B**, Mantel-Cox analysis in **G** and Kruskal-Wallis test with Dunn's post hoc test in **H**. ns; not significant.

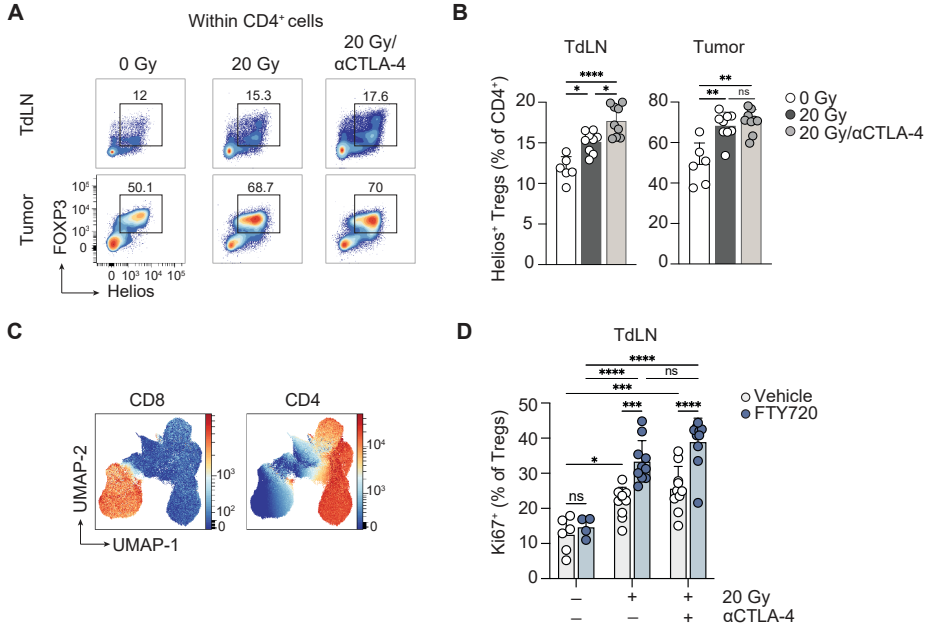

Supplementary Figure 6 – Related to Figure 4.
(A-C) Mice bearing 20 mm^2 TC-1 tumors received RT (20 Gy, n=9) or control (0 Gy, n=6) on day 0. Treatment included vehicle (PBS) or a CTLA-4 blocking mAb on day 0, 3 and 6. The Treg response was measured by flow cytometry in the indicated tissues on day 8. **(A)** Representative concatenated flow cytometry plots and **(B)** quantification depicting the frequency of Helios$^+$ Tregs among CD4$^+$ T cells in the TdLN and tumor. **(C)** UMAP visualization of the CD8$^+$ cells and CD4$^+$ cells among CD3$^+$ cells, related to **Figure 4, D and E**. **(D)** TC-1 tumor-bearing mice received 20 Gy (n=10/group) or control (0 Gy, n=4-6), with CTLA-4 mAb blockade or vehicle on days 0, 3, and 6, with or without FTY720. Depicted is the frequency of Ki67$^+$ cells among Tregs measured in the TdLN on day 8 post-RT. Data are from one experiment representative of two experiments. Error bars indicate SD. *P < 0.05, **P < 0.01, *** P < 0.001, **** P < 0.0001, Kruskal-Wallis with Dunn's post hoc test in **B**, two-way Anova with Tukey's post hoc test in **D**. ns; not significant.

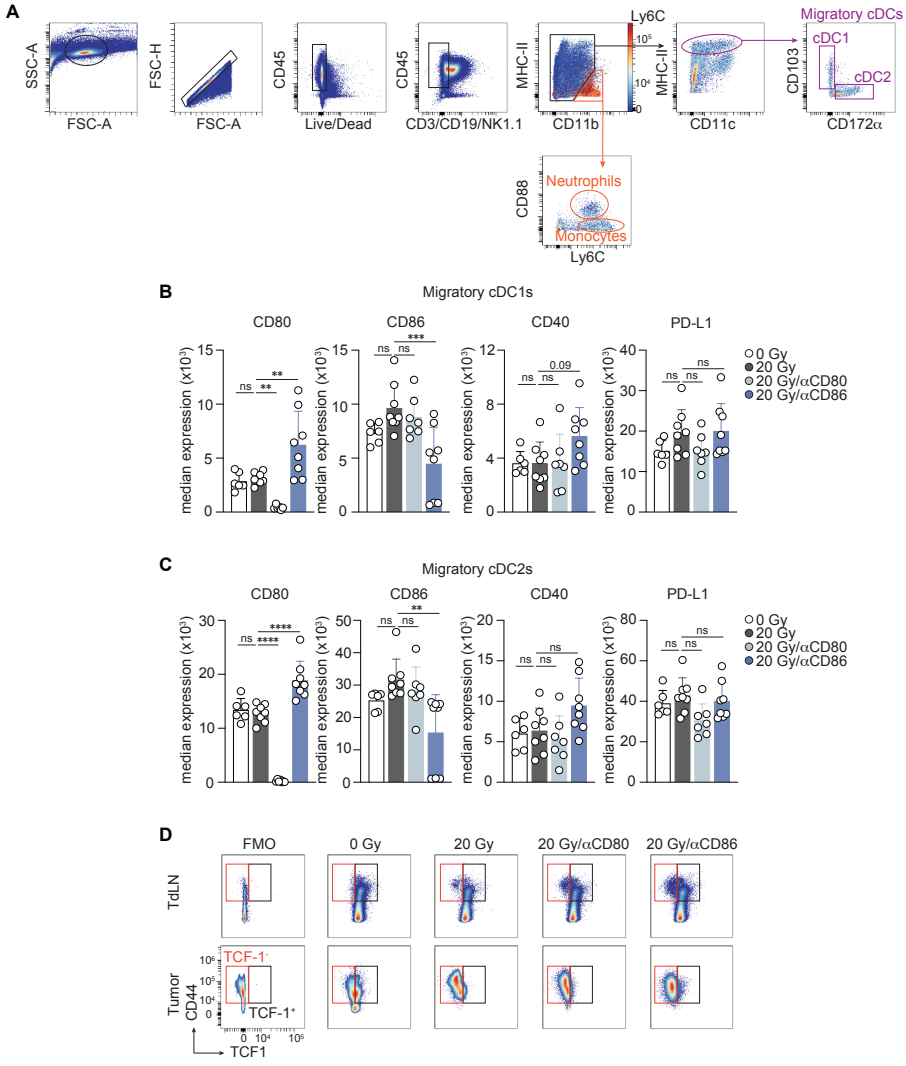

Supplementary Figure 7 – Related to Figure 6.
(A) Representative gating strategy of cDC subsets in the TdLN of TC-1 tumor bearing mice. (B,C) Mice bearing 20 mm^2 TC-1 tumors received control treatment (0 Gy, n=6) or 20 Gy RT at day 0 in combination with either vehicle (PBS, n=8) or blocking mAb against CD80 (n=7) or CD86 (n=8) at day 0, 3 and 6. The cDC response was monitored by flow cytometry in the TdLN at day 8. **(B,C)** Median expression of the indicated markers found on **(B)** migratory cDC1s and **(C)** migratory cDC2s in the TdLN. **(D)** Representative gating strategy of the $CD44^+TCF\text{-}1^-$ cells (orange) and $CD44^+TCF\text{-}1^+$ cells (black) among $CD8^+$ T cells in the TdLN (upper row) and tumor (lower row) for the indicated treatment groups at day 8. FMO; fluorescence minus one. Data are from one experiment representative of two experiments. Error bars indicate SD. **P < 0.01, *** P < 0.001, **** P < 0.0001, ordinary one-way Anova with Dunnett's post hoc test in **C, D**. ns; not significant.

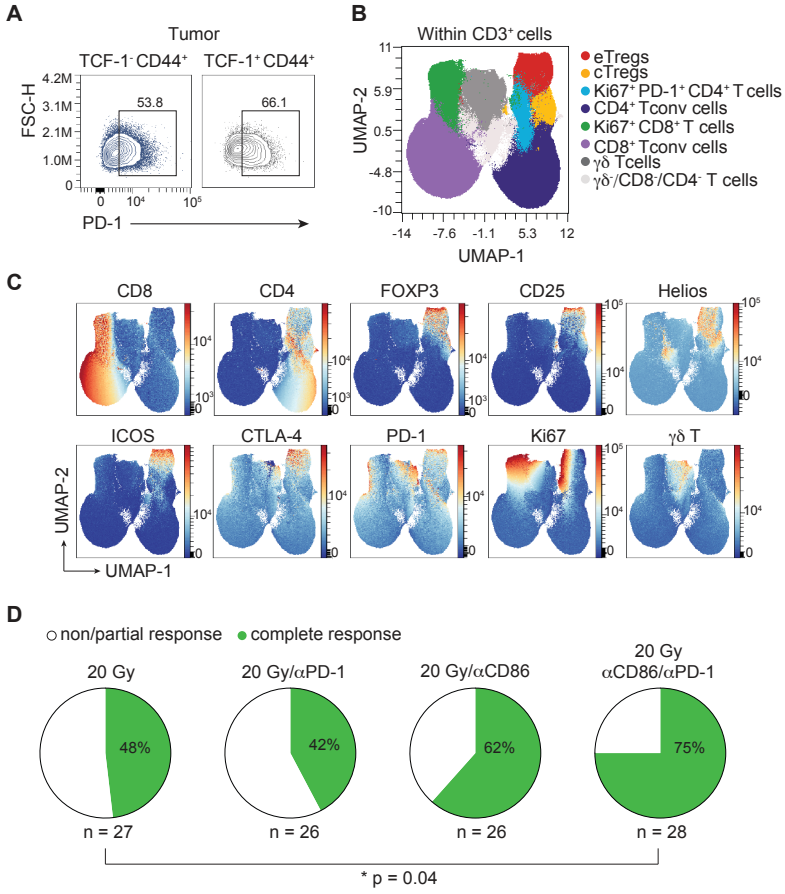

Supplementary Figure 8 – Related to Figure 7.
(A) Mice bearing 20 mm² TC-1 tumors received control treatment (0 Gy, n=5) or 20 Gy RT at day 0 in combination with either vehicle (PBS, n=8) or blocking mAb against CD80 (n=11) or CD86 (n=11) at day 0, 3 and 6. The $CD8^+$ T cell response was monitored by flow cytometry in the tumor at day 8. Representative concatenated (n=11) contour plots are depicted for PD-1 expression on the indicated cell populations among $CD8^+$ T cells in mice treated with 20 Gy and CD86 blockade. Numbers indicate percentages. **(B-C)** Mice bearing TC-1 tumors received control treatment (0 Gy, n=4) or 20 Gy RT at day 0 in combination with either vehicle (PBS, n=8) or blocking mAb against PD-1 (n=11), CD86 (n=10) or a combination of both (n=10) at day 0, 3 and 6. The $CD3^+$ (T-cell) lymphocyte response was monitored by flow cytometry in the non-TdLN, TdLN and tumor at day 8. UMAP display of 2500 randomly selected $CD3^+$ cells per tissue found in non-TdLN, TdLN and tumors at day 8 of all treatment groups combined. FlowSOM guided clustering **(B)** identifying the $CD3^+$ cell populations and **(C)** representative heat map visualization of the markers that identify the $CD3^+$ subpopulations. **(D)** Pie chart depicting the proportion of TC-1 tumor-bearing mice with complete tumor clearance upon treatment with 20 Gy at day 0, in combination with either vehicle (PBS), or blocking mAb against PD-1, CD86 or both CD86 and PD-1 at day 0, 3 and 6. *P<0.05, Chi-square test.

Supplementary Table 1

Flow Cytometry Antibodies

Antigen	*Fluorochrome*	*Clone*	*Vendor*	*Catalog #*
CD11c	BUV496	HL3	BD Biosciences	750483
CD11b	BV510	M1/70	BioLegend	101263
CD19	PerCP Cy5.5	6D5	BioLegend	115534
CD25	BV421	7D4	BD Biosciences	564571
CD3	PerCP Cy5.5	17A2	BD Biosciences	560527
CD3	BV785	17A2	Biolegend	100232
CD3	PE Cy7	145-2C11	eBiosciences	25-0031-81
CD4	BV711	GK1.5	BD Biosciences	563050
CD4	FITC	RM4-4	BioLegend	116003
CD4	BUV395	GK1.5	BD Biosciences	563790
CD40	PE Cy5	3/23	Biolegend	124617
CD43	PE Cy5	1B11	Biolegend	121216
CD44	BV785	IM7	Biolegend	103059
CD45	APC/Fire810	30-F11	BioLegend	103173
CD45	BUV395	30-F11	BD Biosciences	564279
CD45	BUV563	30-F11	BD Biosciences	612924
CD62L	APC/Cy7	MEL-14	BD Biosciences	560514
CD64	AF647	X54-5/7.1	BioLegend	139322
CD8	PerCP Cy5.5	53-6.7	eBiosciences	45-0081-82
CD8	BUV805	53-6.7	BD Biosciences	612898
CD8	AF700	53-6.7	BioLegend	100730
CD80	PE/Dazzle 594	16-10A1	Biolegend	B271480
CD86	BV785	GL-1	Biolegend	B347725
CD103	BV711	M290	BD Biosciences	564320
CD172a	BUV395	P84	BD Biosciences	740282
CTLA-4	BV605	UC10-4B9	BioLegend	106323
CX3CR1	PerCP Cy5.5	SA011F11	Biolegend	B318597
F4/80	BV421	BM8	BioLegend	123137
FOXP3	APC	FJK-16S	eBiosciences	25-5773-82
FOXP3	PE Cy5.5	FJK-16S	eBiosciences	35-5773-80
Granzyme B	PE	GB11	Sanquin	M2289
Helios	PE Cy7	22F6	BioLegend	137235
ICOS	PerCP Cy5.5	C398.4A	BioLegend	313518
IFNγ	eFluor450	XMG-1.2	eBiosciences	48-7311-82
IRF8	APC	V3GYWCH	eBiosciences	17-9852-80
Ki67	AF700	SolA15	eBiosciences	56-5698-82

Flow Cytometry Antibodies				
Ki67	eFluor506	SolA15	eBiosciences	69-5698-80
KLRG1	PE eF610	2F1	Thermo Fisher	4335245
Ly6C	Pacific Blue	HK1.4	BioLegend	128014
MHC-II	APC-eFluor780	M5/114.15.2	eBiosciences	47-5321-80
NK1.1	APC-eF780	PK136	eBiosciences	47-5941-82
NK1.1	PerCP Cy5.5	PK136	BioLegend	108727
PD-1	BUV737	J43	eBiosciences	376-9985-80
PD-L1 (CD274)	BUV737	MIH5	BD Biosciences	741877
TCF-1	APC	C63D9	Cell Signaling Technology	37636S
TCRβ	PE Cy7	H57-597	Biolegend	109222
TCRβ	BUV563	H57-597	BD Biosciences	748406
TNFα	PE Cy7	MP6-XT22	BD Biosciences	561041
γd T cell	BV510	GL3	BioLegend	118131

Viability dyes		
LIVE/DEAD™ Fixable Near-IR Dead Cell Stain Kit	Thermo Fisher	L10119
Zombie UV™ Fixable Viability Kit	Biolegend	423107
Zombie Red™ Fixable Viability Kit	Biolegend	423109

***In vivo* antibodies & reagents**				
Antigen	**Immunogen**	**Clone**	**Vendor**	**Catalog #**
CD25	IgG2a	M2A	Evitria	Gift from S. Quezada (under MTA)
CTLA-4	IgG2a fusion protein	UC10-4F10-11	BioXcell	BE0032
PD-1	Rat IgG2a	RMP1-14	BioXcell	BE0146
CD80	Rat IgG2a	1G10	BioXcell	BE0134
CD86	Rat IgG2a	GL-1	BioXcell	BE0025
CD8	Rat IgG2b	2.43	BioXcell	BE0061
CD4	Rat IgG2b	GK1.5	BioXcell	BE0003-1
FTY720			Cayman Chemical Company	10006292

Supplementary Table 2

TCGA Abbreviation	Cancer Type
ACC	Adrenocortical carcinoma
BLCA	Bladder urothelial carcinoma
BRCA	Breast invasive carcinoma
CESC	Cervical squamous cell carcinoma and endocervical adenocarcinoma
CHOL	Cholangiocarcinoma
COAD	Colon adenocarcinoma
DLBC	Lymphoid Neoplasm Diffuse Large B-cell Lymphoma
ESCA	Esophageal carcinoma
GBM	Glioblastoma multiforme
HNSC	Head and Neck squamous cell carcinoma
KICH	Kidney Chromophobe
KIRC	Kidney renal clear cell carcinoma
KIRP	Kidney renal papillary cell carcinoma
LGG	Brain Lower Grade Glioma
LIHC	Liver hepatocellular carcinoma
LUAD	Lung adenocarcinoma
LUSC	Lung squamous cell carcinoma
MESO	Mesothelioma
OV	Ovarian serous cystadenocarcinoma
PAAD	Pancreatic adenocarcinoma
PCPG	Pheochromocytoma and Paraganglioma
PRAD	Prostate adenocarcinoma
READ	Rectum adenocarcinoma
SARC	Sarcoma
SKCM	Skin Cutaneous Melanoma
STAD	Stomach adenocarcinoma
TGCT	Testicular Germ Cell Tumors
THCA	Thyroid carcinoma
THYM	Thymoma
UCEC	Uterine Corpus Endometrial Carcinoma
UCS	Uterine Carcinosarcoma
UVM	Uveal Melanoma